

Weak-Coupling Limit of the Lattice Nonlinear Schrödinger Integral Equation

Felipe Taha Sant'Ana

Abstract

We study the ground-state integral equation of the quantum lattice nonlinear Schrödinger model—equivalently the isotropic Heisenberg XXX spin chain with spin $s = -1$ —in the weak-coupling limit. Unlike the continuous Lieb–Liniger equation, whose driving term is a constant, the lattice equation is doubly singular: both the driving term and the integral kernel degenerate into δ -functions as $\kappa \rightarrow 0$. We develop a matched asymptotic expansion with three regions—inner, outer, and edge. The Fourier transform of the rescaled inner solution is exactly the Bose–Einstein distribution, and the peak density diverges logarithmically with a constant C , which we determine analytically via two independent routes and confirm numerically. An exact duality with the Love integral equation for the circular disc capacitor yields the total density expansion. We prove an identity for the inner energy, allowing us to obtain the ground-state energy per site. From the Wiener–Hopf factorisation of the edge boundary layer, we identify the instanton action and predict a resurgent transseries structure.

Contents

| | | |
|----------|---|-----------|
| 1 | Introduction | 2 |
| 2 | Lattice nonlinear Schrödinger model | 4 |
| 2.1 | Lattice nonlinear Schrödinger model | 4 |
| 2.2 | Bethe ansatz and thermodynamic limit | 6 |
| 3 | Inner region | 8 |
| 3.1 | Rescaled inner equation | 8 |
| 3.2 | Fourier analysis and logarithmic divergence | 8 |
| 3.3 | Eigenvalue analysis of the truncated kernel | 9 |
| 4 | Outer region and density decomposition | 11 |
| 4.1 | Outer solution and Fermi sea | 11 |
| 4.2 | Duality with the Love integral equation | 11 |
| 4.3 | Total density expansion | 12 |
| 5 | Edge boundary layer | 14 |
| 5.1 | Connection to the capacitor problem | 15 |
| 6 | Determination of C | 16 |
| 6.1 | Mode-counting argument | 16 |
| 6.2 | Wiener–Hopf derivation of the constant | 18 |
| 6.3 | Numerical verification | 20 |
| 7 | Energy and physical predictions | 20 |
| 7.1 | Energy identity | 20 |
| 7.2 | Asymptotic expansion and mode-sum derivation | 21 |
| 7.3 | Ground-state energy | 21 |
| 7.4 | Energy at fixed particle density and comparison with Lieb–Liniger | 22 |

| | | |
|----------|--|-----------|
| 8 | Towards resurgence | 22 |
| 8.1 | Instanton action from the Wiener–Hopf symbol | 22 |
| 8.2 | Spectral gap: algebraic closure with exponential correction | 23 |
| 8.3 | The Fredholm determinant and Szegő asymptotics | 23 |
| 8.4 | Analytical support and connection to the Lieb–Liniger resurgence | 24 |
| 9 | Conclusions | 24 |
| A | Eigenvalue analysis of the truncated kernel | 30 |
| A.1 | Basic spectral properties | 30 |
| A.2 | Resolvent amplification and the origin of logarithmic growth | 32 |
| A.3 | Fredholm determinant and eigenvalue product formula | 33 |
| A.4 | Numerical computation of eigenvalues | 34 |
| B | The total density expansion | 35 |
| C | Wiener–Hopf factorisation | 37 |
| D | Preliminary numerical extraction of perturbative coefficients | 39 |

1 Introduction

The Bethe ansatz, introduced in 1931 for the spin- $\frac{1}{2}$ Heisenberg chain [1], provides exact access to the spectrum and thermodynamics of a wide class of one-dimensional quantum systems. In the thermodynamic limit, the Bethe equations reduce to linear integral equations for the density of quasi-momenta, and the extraction of physical observables—particle density, energy, excitation spectrum—reduces to the analysis of these integral equations in the relevant parameter regimes [2, 3, 4].

The prototypical example is the Lieb–Liniger model [5, 6], describing a one-dimensional Bose gas with repulsive δ -function interactions. In the thermodynamic limit, its ground state is determined by the integral equation

$$2\pi \rho(\lambda) = 1 + \int_{-q}^q K(\lambda - \mu) \rho(\mu) d\mu, \quad K(\lambda) = \frac{2\kappa}{\kappa^2 + \lambda^2}, \quad (1)$$

where $\kappa > 0$ is a coupling parameter and q is the Fermi boundary, determined self-consistently by the particle density. The Yang–Yang thermodynamic formalism [7] extends this to finite temperature. The weak-coupling limit $\kappa \rightarrow 0$ (equivalently $\gamma = c/\rho \rightarrow 0$) has been the subject of extensive study.

Analytical developments of iterative solutions of the integral equation were performed in early work [8] and more recently [9], as well as rigorous results for the ground-state energy [10], while computations of higher-order terms by double extrapolation have also been achieved [11]. Accurate analytical results and conjectures for the excitation spectrum [12], extensions of the expansion to high order and formulation of structural conjectures [13, 14], and the structure of both weak- and strong-coupling expansions for several observables [15] have also been accomplished. These works revealed that the weak-coupling expansion proceeds in half-integer powers of γ , with coefficients involving Riemann zeta values at odd arguments. Subsequently, exact perturbative results and demonstration that the series is not Borel summable were obtained [16], establishing a connection to non-perturbative effects in the dual Gaudin–Yang model [17, 18].

A key mathematical insight [19] is that the Lieb–Liniger integral equation belongs to the same family as the Love integral equation governing the electrostatic potential of two coaxial circular conducting discs [20]. The capacitor problem has a long history in mathematical physics, dating back to Kirchhoff [21] and Maxwell [22], with important contributions in the early twentieth century [23, 24] and thereafter [25, 26, 27]. The small-separation asymptotics of the capacitor, involving logarithmic terms and Wiener–Hopf boundary-layer corrections, are directly relevant to the weak-coupling analysis of the Bethe ansatz. Recently, [28] provided a comprehensive survey of Love–Lieb integral

equations, unifying the electrostatic and quantum-mechanical perspectives. Moreover, analytical results for the capacitance have been obtained [29], as well as extension of the Wiener–Hopf analysis to study non-perturbative corrections for the disc capacitor and the $O(N)$ free energy [30].

The discovery that the Lieb–Liniger expansion is non-Borel summable [16] sparked a programme of resurgent analysis in integrable quantum field theories. The key tool is the Wiener–Hopf factorisation of the integral equation’s symbol (developed in this context in [31, 32]), which gives systematic access to both perturbative and non-perturbative sectors. Extending such an analysis to renormalons in integrable field theories has also been the subject of investigation [33, 34], not to mention the Hubbard model [35], and the energy gap problem [36]. Important developments were carried out on the $1/N$ expansion [37] and detailed analyses of the $O(4)$ and $O(3)$ sigma models [38, 39, 40]. More recently, Bajnok, Balog, and Vona [41] obtained the complete transseries for conserved charges. These developments are reviewed in [42, 43].

The quantum inverse scattering method (QISM) [44, 45] provides the algebraic framework for constructing integrable quantum models on the lattice (see also [46, 47, 48, 49] for reviews). The quantum nonlinear Schrödinger (NLS) model on a lattice was constructed within this framework [50, 51, 52, 45], with local Hamiltonians worked out in [53]. The lattice NLS provides an integrable discretisation of the continuous NLS field theory, preserving the full integrability structure at the quantum level [3, 54]. The model is closely related to the q -boson hopping model [55] and it was diagonalised in [56], while Dorlas [57] established completeness of the Bethe ansatz eigenstates for the NLS model.

The lattice NLS model is equivalent to the isotropic Heisenberg XXX spin chain with spin $s = -1$, in the sense of the negative-spin representations recently introduced [58]. The thermodynamics of this chain was also studied recently [59]. The higher-spin XXX chain has been solved [60, 61]. The negative-spin case extends this to non-compact representations, connecting to the $SL(2, \mathbb{R})$ spin chains that appear in high-energy QCD [62, 63, 64, 65]. Non-compact spin chains have also been studied as integrable stochastic processes [66], and the thermodynamic limit of $SL(2, \mathbb{C})$ chains was analysed too [67].

The same integral equation (2) appears in high-energy quantum chromodynamics: the $\kappa \rightarrow 0$ limit of the $XXX_{s=-1}$ chain corresponds to the weak-coupling/high-density regime of reggeized gluon dynamics. Furthermore, it was discovered [68, 69, 70, 71] that the BFKL pomeron equation—governing small- x parton evolution [72, 73, 74, 75]—possesses a hidden integrable structure equivalent to a non-compact Heisenberg spin chain. Faddeev and Korchemsky [76] proved the complete integrability of the BFKL Hamiltonian and identified it with the $XXX_{s=0}$ spin chain, while Korchemsky [77, 78, 79] developed the Bethe ansatz for the QCD pomeron and studied its quasiclassical limit (see also [80, 81] for reviews). Finally, de Vega and Lipatov [82] extended the analysis to multi-reggeon interactions. In this context, the logarithmic scaling we find is qualitatively consistent with the logarithmic energy dependence characteristic of BFKL dynamics, though a precise quantitative comparison requires further work (see Section 2).

The ground-state integral equation of the lattice NLS model reads

$$2\pi \rho(\lambda) = K(\lambda) + \int_{-q}^q K(\lambda - \mu) \rho(\mu) d\mu. \quad (2)$$

The crucial difference from (1) is that the driving term is now the Lorentzian $K(\lambda)$ —itself degenerating into $2\pi\delta(\lambda)$ as $\kappa \rightarrow 0$ —rather than the constant 1. This makes the weak-coupling limit doubly singular: both the driving term and the kernel collapse into δ -functions simultaneously, and the techniques developed for the Lieb–Liniger case—which exploit the regularity of the constant driving term—do not directly apply.

In this paper we develop a systematic matched asymptotic expansion for equation (2) as $\kappa \rightarrow 0$, exploiting three distinct regions of the rescaled spectral variable $\xi = \lambda/\kappa$. The methods draw on classical techniques of singular perturbation theory [83, 84, 85, 86] and on the Wiener–Hopf factorisation technique [87, 88, 89] as applied to convolution integral equations on finite intervals [90]. The matched asymptotic expansion is formal in the sense of classical singular perturbation theory; the leading-order results are confirmed analytically by the Wiener–Hopf derivation of Section 6.2

and verified numerically throughout. Our main findings are: i) in the inner region ($|\xi| \lesssim 1$), the equation reduces to a Lieb–Liniger-type equation on the expanding domain $[-Q, Q]$ with $Q = q/\kappa \rightarrow \infty$. On the full line, the Fourier transform of the rescaled solution is exactly the Bose–Einstein distribution $\hat{\rho}(p) = 1/(e^{|p|} - 1)$ —a function familiar from the Yang–Yang thermodynamic Bethe ansatz [7, 91]—whose infrared singularity produces a logarithmic divergence at the origin. We determine the constant analytically as $C = (\gamma_E + \log 2)/\pi$ via two independent routes: a mode-counting argument combined with a digamma representation of the solution, and a direct Wiener–Hopf derivation using the spectral response function of the truncated operator. Both are confirmed numerically by Richardson extrapolation; ii) in the outer region ($1 \ll |\xi| \ll Q$), the solution reduces to a uniform Fermi sea with $\tilde{\rho}_{\text{bulk}} = 1/2$, which dominates the total density. Using a duality with the Love integral equation [20, 28], together with the self-consistency identity $f(0) = 1 + D(Q)$ and a novel integral identity for the digamma function, we derive the total density expansion $D(Q) = Q + (2\pi)^{-1} \log Q + b + \dots$; iii) In the edge boundary layer of width $\mathcal{O}(1)$ in the rescaled variable near $\xi = \pm Q$, the equation reduces to a half-line Wiener–Hopf problem with symbol $\Sigma = 1 - e^{-|p|}$. We obtain the factorisation of this symbol in terms of gamma functions and identify the Wiener–Hopf constant $A_{\text{WH}} = 2$. The structure of the edge problem is closely related to the Kirchhoff–Maxwell analysis of fringing fields in the circular disc capacitor [21, 26, 28, 30]; iv) We prove the identity $E_{\text{inner}}(Q) = 2\pi\tilde{\rho}(0; Q) - 2$, valid for all $Q > 0$, which reduces the energy calculation to the peak density. The physical ground-state energy per site is then $e(\kappa) = -2[\log(2q/\kappa) + \gamma_E - 1]/\kappa + \dots$, scaling as $e(\kappa) \sim -2\log(1/\kappa)/\kappa$ —qualitatively different from the Lieb–Liniger energy $e(\gamma) \sim \gamma$ at weak coupling. All analytical predictions are confirmed by numerical computations.

The paper is organised as follows. Section 2 introduces the model, its Bethe ansatz solution, and the resulting integral equation. Section 3 develops the inner-region analysis, deriving the Bose–Einstein distribution and the logarithmic divergence. Section 4 treats the outer region and derives the density expansion. Section 5 describes the edge boundary layer. Section 6 determines the constant C analytically and discusses its Wiener–Hopf interpretation. Section 7 derives the ground-state energy via an exact identity and discusses the physical predictions, including the comparison with the Lieb–Liniger model. Section 8 presents analytical predictions for the resurgent structure. Section 9 summarises the results and discusses open problems. The appendices contain further analytical and numerical details: eigenvalue analysis of the truncated kernel (Appendix A), the total density expansion (Appendix B), the Wiener–Hopf factorisation (Appendix C), and preliminary numerical extraction of perturbative coefficients (Appendix D).

2 Lattice nonlinear Schrödinger model

We now provide the fundamentals of the lattice nonlinear Schrödinger model, explain its equivalence to the isotropic Heisenberg XXX spin chain with spin $s = -1$, derive the Bethe ansatz equations, and take the thermodynamic limit to obtain the integral equation (2), which is the central object of the paper.

2.1 Lattice nonlinear Schrödinger model

The algebraic Bethe ansatz, or quantum inverse scattering method (QISM) [44, 45, 46, 47, 48, 49], constructs integrable quantum lattice models from solutions of the Yang–Baxter equation. The starting point is an R-matrix $R(\lambda) \in \text{End}(\mathbb{C}^2 \otimes \mathbb{C}^2)$ satisfying the Yang–Baxter equation

$$R_{12}(\lambda - \mu) R_{13}(\lambda) R_{23}(\mu) = R_{23}(\mu) R_{13}(\lambda) R_{12}(\lambda - \mu) \quad (3)$$

in $\text{End}(\mathbb{C}^2 \otimes \mathbb{C}^2 \otimes \mathbb{C}^2)$. For the models of interest here, the R-matrix is the rational (XXX-type) solution

$$R(\lambda) = \lambda \mathbf{I} + i \mathbf{P}, \quad (4)$$

where \mathbf{I} is the identity and \mathbf{P} is the permutation operator on $\mathbb{C}^2 \otimes \mathbb{C}^2$. Explicitly, in the standard basis,

$$R(\lambda) = \begin{pmatrix} \lambda + i & 0 & 0 & 0 \\ 0 & \lambda & i & 0 \\ 0 & i & \lambda & 0 \\ 0 & 0 & 0 & \lambda + i \end{pmatrix}. \quad (5)$$

The construction of an integrable model on a lattice of M sites proceeds by choosing, at each site n , a local Lax operator $L_n(\lambda) \in \text{End}(\mathbb{C}^2 \otimes \mathcal{H}_n)$, where \mathbb{C}^2 is the auxiliary space and \mathcal{H}_n is the local quantum space at site n . The Lax operator must satisfy the intertwining relation

$$R_{12}(\lambda - \mu) L_{1n}(\lambda) L_{2n}(\mu) = L_{2n}(\mu) L_{1n}(\lambda) R_{12}(\lambda - \mu), \quad (6)$$

which ensures that the monodromy matrix

$$T(\lambda) = L_M(\lambda) L_{M-1}(\lambda) \cdots L_1(\lambda) =: \begin{pmatrix} A(\lambda) & B(\lambda) \\ C(\lambda) & D(\lambda) \end{pmatrix} \quad (7)$$

satisfies the RTT relation

$$R_{12}(\lambda - \mu) T_1(\lambda) T_2(\mu) = T_2(\mu) T_1(\lambda) R_{12}(\lambda - \mu). \quad (8)$$

The transfer matrix $\tau(\lambda) = \text{tr}_{\mathbb{C}^2} T(\lambda) = A(\lambda) + D(\lambda)$ then generates a commuting family: $[\tau(\lambda), \tau(\mu)] = 0$ for all λ, μ . The Hamiltonian and higher conserved charges are extracted from the logarithmic derivative of $\tau(\lambda)$ at a reference point [53, 3].

The lattice NLS model was constructed within the QISM framework [50, 51, 52, 45] with local Hamiltonians worked out in [53]. The local quantum space at each site is a bosonic Fock space $\mathcal{H}_n = \text{span}\{|0\rangle_n, |1\rangle_n, |2\rangle_n, \dots\}$, with creation and annihilation operators ψ_n^\dagger, ψ_n satisfying $[\psi_n, \psi_m^\dagger] = \delta_{nm}$ and number operator $N_n = \psi_n^\dagger \psi_n$.

The Lax operator for the lattice NLS model is [50, 3]

$$L_n(\lambda) = \begin{pmatrix} \lambda - i\kappa N_n/2 & i\sqrt{\kappa} \psi_n^\dagger \\ i\sqrt{\kappa} \psi_n & 1 \end{pmatrix}, \quad (9)$$

where $\kappa > 0$ is the coupling constant (related to the lattice spacing in the continuous limit). One verifies that (9) satisfies the intertwining relation (6) with the rational R-matrix (4). The parameter κ controls the interaction strength: in the limit $\kappa \rightarrow 0$ (with appropriate rescaling), the model reduces to the continuous quantum NLS field theory [3, 54].

The Hamiltonian, obtained from $\tau(\lambda)$ via [53]

$$H = i\kappa \left. \frac{d}{d\lambda} \log \tau(\lambda) \right|_{\lambda=i\kappa/2} + \text{const}, \quad (10)$$

takes the form of a nearest-neighbour hopping model with nonlinear (density-dependent) interactions:

$$H = - \sum_{n=1}^M \left(\psi_{n+1}^\dagger \psi_n + \psi_n^\dagger \psi_{n+1} \right) + \frac{\kappa}{2} \sum_{n=1}^M N_n(N_n - 1) + \text{boundary terms}. \quad (11)$$

The first term is the hopping (kinetic energy), and the second is the on-site repulsive interaction. The connection between the lattice NLS model and the higher-spin Heisenberg chain arises from the representation theory of $\mathfrak{sl}(2)$.

The isotropic Heisenberg XXX spin chain with spin s [60, 61] is constructed by choosing the local quantum space \mathcal{H}_n to be the $(2s + 1)$ -dimensional irreducible representation of $\mathfrak{sl}(2)$ (for $s = 1/2, 1, 3/2, \dots$). The Lax operator is

$$L_n^{(s)}(\lambda) = \lambda \mathbf{I} + i \sum_{\alpha=1}^3 \sigma_\alpha \otimes S_n^\alpha, \quad (12)$$

where σ_α are the Pauli matrices (acting on the auxiliary \mathbb{C}^2) and S_n^α are the spin- s generators of $\mathfrak{sl}(2)$ at site n . For $s = 1/2$, this recovers the original Heisenberg model [1].

Observe that the Lax operator (12) can be analytically continued to non-integer and even negative values of s , provided one works with infinite-dimensional representations of $\mathfrak{sl}(2)$ [58]. For $s = -1$, the representation is realised on the bosonic Fock space $\mathcal{H}_n = \text{span}\{|k\rangle_n : k = 0, 1, 2, \dots\}$ via the generators

$$S_n^+ = \psi_n^\dagger, \quad S_n^- = -N_n \psi_n, \quad S_n^z = -N_n - \frac{1}{2}, \quad (13)$$

which satisfy the $\mathfrak{sl}(2)$ commutation relations $[S^z, S^\pm] = \pm S^\pm$, $[S^+, S^-] = 2S^z$, with $\mathbf{S}^2 = s(s+1) = 0$. Substituting into (12) with the identification $\kappa \leftrightarrow 1$ (after a gauge transformation and reparametrisation of the spectral parameter), one recovers (9) up to an overall scalar factor.

The precise equivalence is [58, 59]:

$$\text{Lattice NLS model with coupling } \kappa \equiv \text{XXX spin chain with spin } s = -1 \text{ and } \kappa = 1, \quad (14)$$

where the coupling κ in the lattice NLS plays the role of a parametrisation of the spectral parameter in the spin-chain language. More precisely, the spin-chain Lax operator (12) with $s = -1$ is defined at $\kappa = 1$; arbitrary κ is recovered by the rescaling $\lambda \rightarrow \lambda/\kappa$ of the spectral parameter, which leaves the Yang–Baxter equation invariant but rescales the kernel in the Bethe ansatz equations (16) by κ . The infinite-dimensional local Hilbert space (bosonic Fock space) is the hallmark of the non-compact ($s < 0$) representations, in contrast to the finite-dimensional spaces of the standard higher-spin chains.

The same non-compact $\mathfrak{sl}(2)$ representations appear in the integrable structures of high-energy quantum chromodynamics [68, 69, 70, 71]. [76] proved that the BFKL pomeron Hamiltonian—governing the small- x evolution of parton distributions [72, 73, 74, 75]—is equivalent to the Hamiltonian of a non-compact Heisenberg spin chain with $\mathfrak{sl}(2, \mathbb{R})$ symmetry, and [77, 78, 79] developed the Bethe ansatz for this QCD spin chain (see also [80, 81] for reviews). Our integral equation (2) governs the ground state in the high-density regime, and the logarithmic scaling $\tilde{\rho}(0; Q) \sim (\log Q)/\pi$ that we find is qualitatively consistent with the $\log(1/x)$ dependence characteristic of BFKL dynamics. However, since the BFKL pomeron corresponds to spin $s = 0$ in the Faddeev–Korchemsky identification [76] whereas our model has $s = -1$, a precise quantitative mapping requires a careful continuation in the spin parameter, which is left for future work.

2.2 Bethe ansatz and thermodynamic limit

The algebraic Bethe ansatz diagonalises the transfer matrix $\tau(\lambda)$ by constructing eigenstates of the form

$$|\{\lambda_j\}\rangle = \prod_{j=1}^N B(\lambda_j) |0\rangle, \quad (15)$$

where $|0\rangle = |0\rangle_1 \otimes \dots \otimes |0\rangle_M$ is the Fock vacuum (all sites empty), $B(\lambda)$ is the off-diagonal element of monodromy matrix (7), and N is the number of particles. The state (15) is an eigenstate of $\tau(\lambda)$ provided the rapidities $\{\lambda_j\}_{j=1}^N$ satisfy the Bethe ansatz equations (BAE) [3, 58, 59]:

$$\left(\frac{\lambda_j + i\kappa/2}{\lambda_j - i\kappa/2} \right)^M = \prod_{\substack{k=1 \\ k \neq j}}^N \frac{\lambda_j - \lambda_k + i\kappa}{\lambda_j - \lambda_k - i\kappa}, \quad j = 1, \dots, N. \quad (16)$$

The energy eigenvalue is extracted via (10) [53, 3]:

$$E = - \sum_{j=1}^N \frac{\kappa^2}{\lambda_j^2 + \kappa^2/4} + \text{const.} \quad (17)$$

We now take the thermodynamic limit $M, N \rightarrow \infty$ with fixed density $D = N/M$ and fixed coupling κ . In this limit, the Bethe roots $\{\lambda_j\}$ become dense on an interval $[-q, q]$ (the Fermi sea), with a distribution function $\rho(\lambda)$ normalised so that

$$\int_{-q}^q \rho(\lambda) d\lambda = D = \frac{N}{M}. \quad (18)$$

The Fermi boundary q is determined self-consistently by the particle density.

Taking the logarithm of the BAE (16) and passing to the continuum, the ground-state integral equation for the lattice NLS model becomes (cf. (2) in the introduction):

$$2\pi \rho(\lambda) = \frac{2\kappa}{\kappa^2 + \lambda^2} + \int_{-q}^q \frac{2\kappa}{\kappa^2 + (\lambda - \mu)^2} \rho(\mu) d\mu, \quad (19)$$

where the Lorentzian kernel is $K(\lambda; \kappa) = 2\kappa/(\kappa^2 + \lambda^2)$, normalised so that $\int_{-\infty}^{\infty} K(\lambda; \kappa) d\lambda = 2\pi$ for all $\kappa > 0$. This is a Fredholm integral equation of the second kind on the symmetric interval $[-q, q]$, with a Lorentzian kernel that is symmetric, positive, and of convolution type.

The crucial structural difference from the Lieb–Liniger integral equation (1) lies in the driving term: in the Lieb–Liniger equation, the driving term is the constant 1, arising from the unrestricted quadratic dispersion of the continuous model; in the lattice NLS equation (19), the driving term is the Lorentzian $K(\lambda; \kappa)$, reflecting the bounded bandwidth of the lattice momentum. In the limit $\kappa \rightarrow 0$, $K(\lambda; \kappa) \rightarrow 2\pi \delta(\lambda)$ in the distributional sense, so the driving term degenerates into a δ -function. This is the source of the doubly singular structure that makes the weak-coupling analysis of (19) qualitatively different from that of (1). This singular behaviour necessitates the matched asymptotic expansion developed in the following sections¹.

Once the density $\rho(\lambda)$ is known, the physical observables of the ground state are computed as follows. The number of particles per site is

$$D = \int_{-q}^q \rho(\lambda) d\lambda. \quad (21)$$

The energy per site in the thermodynamic limit follows from (17):

$$e(\kappa) = - \int_{-q}^q \frac{2\kappa}{\kappa^2 + \lambda^2} \rho(\lambda) d\lambda = - \int_{-q}^q K(\lambda; \kappa) \rho(\lambda) d\lambda. \quad (22)$$

The kernel appearing in the energy integral is the same function $K(\lambda; \kappa)$ that serves as both the driving term and the scattering kernel in (19)—a coincidence specific to the lattice NLS model that will have important consequences². The total momentum per site is $P = 0$ for the ground state, by parity. Excited states are described by particle–hole excitations above the Fermi sea, with dressed energy and dressed momentum satisfying linear integral equations of the same type as (19), with different driving terms [3, 7]. The excitation spectrum and thermodynamics of the $\text{XXX}_{s=-1}$ chain were recently studied [59]. In this manuscript, we restrict ourselves to the ground-state.

¹The kernel $K(\lambda - \mu; \kappa)$ and the driving term $K(\lambda; \kappa)$ are both even functions, so the solution $\rho(\lambda)$ is even: $\rho(-\lambda) = \rho(\lambda)$. Since $K \geq 0$ and the driving term $K > 0$, the Neumann series converges and $\rho(\lambda) > 0$ for all $\lambda \in [-q, q]$ [3]. The Fourier transform of the Lorentzian kernel is

$$\hat{K}(p; \kappa) = \int_{-\infty}^{\infty} e^{-ip\lambda} \frac{2\kappa}{\kappa^2 + \lambda^2} d\lambda = 2\pi e^{-\kappa|p|}. \quad (20)$$

This exponential decay in momentum space is crucial: the kernel is almost critical in the sense that $\hat{K}(0; \kappa) = 2\pi$ equals the prefactor on the left-hand side of (19), making the homogeneous equation $2\pi\rho = K * \rho$ have eigenvalue 1 on the full line. On the finite interval $[-q, q]$, the largest eigenvalue is strictly less than 2π , but approaches it as $q/\kappa \rightarrow \infty$ —which is precisely the weak-coupling limit.

²See the identity $E_{\text{inner}} = 2\pi\tilde{\rho}(0) - 2$ in Section 7

3 Inner region

3.1 Rescaled inner equation

To resolve the singularity, we introduce the rescaled variables

$$\xi = \frac{\lambda}{\kappa}, \quad \tilde{\rho}(\xi) = \kappa \rho(\kappa\xi), \quad Q = \frac{q}{\kappa}, \quad (23)$$

which “zoom in” on the region $|\lambda| \sim \kappa$ where the driving term is concentrated. Note that the rescaling preserves the particle density:

$$\int_{-Q}^Q \tilde{\rho}(\xi) d\xi = \int_{-q}^q \rho(\lambda) d\lambda = D, \quad (24)$$

since $\tilde{\rho}(\xi) d\xi = \kappa \rho(\kappa\xi) \cdot d\lambda/\kappa = \rho(\lambda) d\lambda$. Under this change of variables, equation (19) becomes

$$2\pi \tilde{\rho}(\xi) = \frac{2}{1 + \xi^2} + \int_{-Q}^Q \frac{2}{1 + (\xi - \eta)^2} \tilde{\rho}(\eta) d\eta. \quad (25)$$

This is a Lieb–Liniger-type equation on the expanding domain $[-Q, Q]$, but with the constant driving term 1 replaced by the Lorentzian

$$K(\xi) = \frac{2}{1 + \xi^2} \quad (26)$$

and the coupling parameter set to $\kappa = 1$. The limit $\kappa \rightarrow 0$ at fixed q corresponds to $Q = q/\kappa \rightarrow \infty$.

The physical observables transform as:

$$D = \int_{-Q}^Q \tilde{\rho}(\xi) d\xi, \quad e(\kappa) = -\frac{1}{\kappa} \int_{-Q}^Q \frac{2}{1 + \xi^2} \tilde{\rho}(\xi) d\xi. \quad (27)$$

The analysis of (25) as $Q \rightarrow \infty$ is the subject of the remainder of this paper.

In the weak-coupling limit $\kappa \rightarrow 0$ we work with the rescaled inner variables (23). In the limit $Q \rightarrow \infty$, the integration domain can be extended to the whole real line, and the inner equation (25) takes the convolution form

$$2\pi \tilde{\rho}(\xi) = g(\xi) + (K * \tilde{\rho})(\xi), \quad (28)$$

where

$$g(\xi) = K(\xi), \quad (K * \tilde{\rho})(\xi) = \int_{-\infty}^{\infty} K(\xi - \eta) \tilde{\rho}(\eta) d\eta. \quad (29)$$

3.2 Fourier analysis and logarithmic divergence

We use the Fourier transform convention

$$\widehat{f}(p) = \int_{-\infty}^{\infty} e^{-ip\xi} f(\xi) d\xi, \quad f(\xi) = \frac{1}{2\pi} \int_{-\infty}^{\infty} e^{ip\xi} \widehat{f}(p) dp, \quad (30)$$

so that the Fourier transform of a convolution is the product of Fourier transforms. The standard integral

$$\int_{-\infty}^{\infty} \frac{e^{-ip\xi}}{1 + \xi^2} d\xi = \pi e^{-|p|} \quad (31)$$

implies

$$\widehat{K}(p) = \widehat{g}(p) = 2\pi e^{-|p|}. \quad (32)$$

Applying the Fourier transform to the full-line equation yields

$$2\pi \widehat{\tilde{\rho}}(p) = 2\pi e^{-|p|} + 2\pi e^{-|p|} \widehat{\tilde{\rho}}(p), \quad (33)$$

where the convolution theorem has been used. Solving algebraically:

$$\hat{\rho}(p) = \frac{e^{-|p|}}{1 - e^{-|p|}} = \frac{1}{e^{|p|} - 1}. \quad (34)$$

This is the Bose–Einstein distribution. It presents a $1/|p|$ singularity at $p = 0$:

$$\frac{1}{e^{|p|} - 1} = \frac{1}{|p|} - \frac{1}{2} + \frac{|p|}{12} + \mathcal{O}(|p|^3). \quad (35)$$

Consequently, the inverse Fourier transform

$$\tilde{\rho}^{(\infty)}(\xi) = \frac{1}{\pi} \int_0^\infty \frac{\cos(\xi p)}{e^p - 1} dp \quad (36)$$

diverges logarithmically at $\xi = 0$. This divergence is regularised by the finite domain $[-Q, Q]$, producing the logarithmic dependence on Q .

To isolate the divergence we introduce a lower cutoff $\varepsilon > 0$ and consider

$$I(\varepsilon) = \int_\varepsilon^\infty dp \frac{1}{e^p - 1}. \quad (37)$$

Using the geometric series

$$\frac{1}{e^p - 1} = \sum_{n=1}^\infty e^{-np} \quad (38)$$

and integrating term by term, we obtain

$$I(\varepsilon) = \sum_{n=1}^\infty e^{-n\varepsilon}/n = -\log(1 - e^{-\varepsilon}). \quad (39)$$

For small ε ,

$$I(\varepsilon) = -\log \varepsilon + \mathcal{O}(1), \quad \varepsilon \rightarrow 0. \quad (40)$$

In summary, the Bose integral produces a universal logarithmic divergence, reflecting the $1/|p|$ singularity at $p = 0$. In the finite-domain equation, the divergence is regulated by the finite spatial interval $[-Q, Q]$.

3.3 Eigenvalue analysis of the truncated kernel

The integral operator \mathcal{K}_Q on $L^2([-Q, Q])$ defined by

$$(\mathcal{K}_Q f)(\xi) = \int_{-Q}^Q \frac{2}{1 + (\xi - \eta)^2} f(\eta) d\eta \quad (41)$$

has a discrete spectrum $\{\lambda_n(Q)\}_{n=0}^\infty$ with $\lambda_0(Q) > \lambda_1(Q) > \dots > 0$.

On the full line, $\hat{\mathcal{K}}(p) = 2\pi e^{-|p|}$, meaning that the operator norm is 2π . For finite Q , the largest eigenvalue $\lambda_0(Q)$ approaches 2π from below: $\lambda_0(Q) = 2\pi - \Delta(Q)$, with $\Delta(Q) \rightarrow 0$ as $Q \rightarrow \infty$. The spectral gap $\Delta(Q)$ controls the divergence rate of the solution: near the critical eigenvalue, the resolvent $(2\pi I - \mathcal{K}_Q)^{-1}$ amplifies the driving term by a factor $\sim 1/\Delta(Q) \sim \log Q$, producing the asymptotic growth

$$\tilde{\rho}(0; Q) = \frac{\log Q}{\pi} + C + o(1), \quad (42)$$

where C is a constant determined by the detailed structure of the finite-interval problem, including the boundary layers near $\xi = \pm Q$. Further analytical details on the spectral properties of \mathcal{K}_Q are given in Appendix A; the closing of the spectral gap is illustrated in Figure 2. The integral equation (25) is also closely related to the classical Love integral equation [20] for the circular disc capacitor; this connection, and the resulting duality that links the lattice NLS density to the Love solution, is developed in detail in Section 4.2.

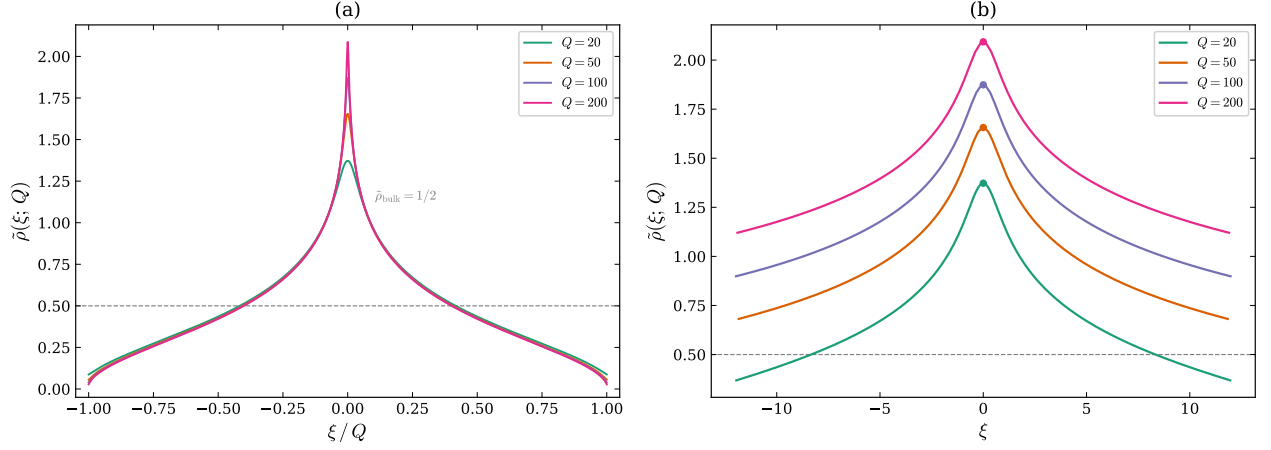


Figure 1: Numerical solution of the rescaled integral equation (25) for $Q = 20, 50, 100$, and 200 . **(a)** Rescaled density $\tilde{\rho}(\xi; Q)$ plotted against ξ/Q , showing the full domain $[-Q, Q]$. All curves share the same outer-region (Fermi-sea) plateau at $\tilde{\rho}_{\text{bulk}} = 1/2$ (dashed line), while the central Bose–Einstein peak grows logarithmically with Q . The edge boundary layers at $\xi/Q = \pm 1$ are visible as the rapid drop from the plateau to zero. **(b)** Zoom into the inner region $|\xi| \lesssim \mathcal{O}(1)$, plotted against the unscaled variable ξ . The peak height at $\xi = 0$ increases as $\tilde{\rho}(0; Q) \sim (\log Q)/\pi + C$ (see (42)), with the logarithmic growth clearly visible across the four values of Q . The cusp-like shape reflects the $1/|p|$ infrared singularity of the Bose–Einstein distribution (34) in Fourier space, and the universal profile is controlled by the digamma function $\text{Re } \psi(1 + i\xi)$. In panel (b), the dashed curves show the analytical inner approximation $\tilde{\rho}(\xi; Q) \approx [\log(2Q) - \text{Re } \psi(1 + i\xi)]/\pi$ from (45), which matches the numerical solution to graphical accuracy for $|\xi| \lesssim Q/2$.

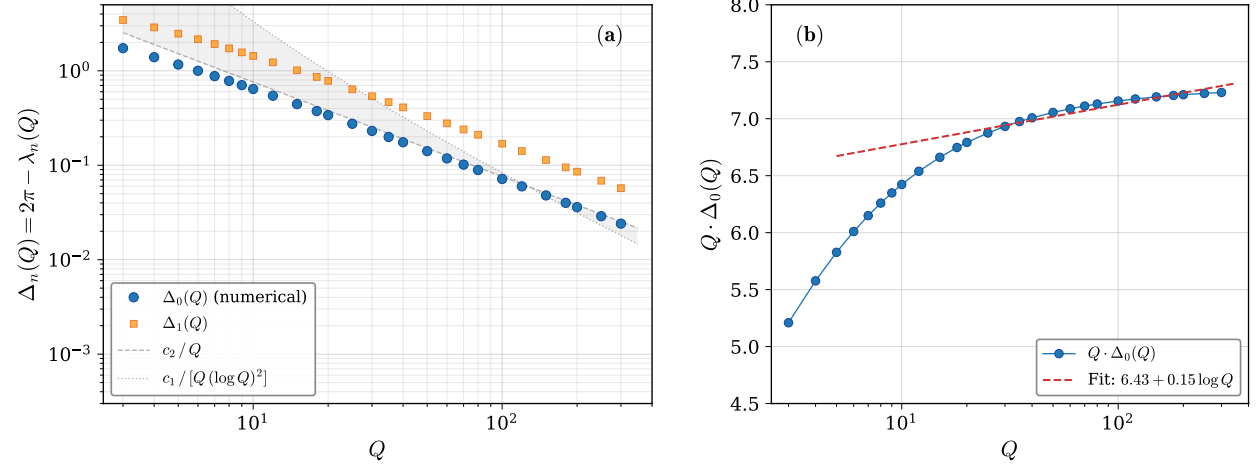


Figure 2: Spectral gap of the truncated kernel \mathcal{K}_Q . **(a)** Log–log plot of $\Delta_n(Q) = 2\pi - \lambda_n(Q)$ for $n = 0$ (circles) and $n = 1$ (squares) versus Q . The shaded region indicates the proven bounds $c_1/[Q(\log Q)^2] \leq \Delta_0(Q) \leq c_2/Q$. Both gaps close algebraically, with Δ_0 separated below Δ_1 for all Q . **(b)** Compensated gap $Q \cdot \Delta_0(Q)$ versus Q on a semi-logarithmic scale. If Δ_0 scaled as $1/Q$, the product $Q \cdot \Delta_0$ would be constant; instead, it grows slowly, well fitted by $Q \cdot \Delta_0 \approx 6.43 + 0.15 \log Q$ (dashed line), confirming the logarithmic correction to the $1/Q$ law.

4 Outer region and density decomposition

4.1 Outer solution and Fermi sea

For $\kappa \ll |\lambda| \ll q$ (equivalently $1 \ll |\xi| \ll Q$ in the rescaled variable), the driving term $g(\xi) = 2/(1 + \xi^2) \approx 2/\xi^2$ is small, and the equation becomes approximately homogeneous:

$$2\pi\tilde{\rho} \approx \mathcal{K}_Q\tilde{\rho}. \quad (43)$$

Since $\int_{-\infty}^{\infty} K(x) dx = 2\pi$ and the solution varies slowly on the $\mathcal{O}(1)$ scale of the kernel, the convolution integral evaluates to $\approx 2\pi\tilde{\rho}$, and the equation is trivially satisfied for any constant $\tilde{\rho}$.

The specific value of the constant is selected by the spectral structure of the truncated operator. The largest eigenvalue of the Love operator $\mathcal{L}_Q = (2\pi)^{-1}\mathcal{K}_Q$ satisfies $\mu_0(Q) \rightarrow 1^-$ with spectral gap $\delta(Q) = 1 - \mu_0(Q) \rightarrow 0$. The associated eigenfunction $\varphi_0(\xi) \approx (2Q)^{-1/2}$ is approximately constant on $[-Q, Q]$. Projecting the inhomogeneous equation onto this near-critical mode and requiring self-consistency ($D \sim 2Q\tilde{\rho}_{\text{bulk}} \sim Q$) yields

$$\tilde{\rho}_{\text{bulk}} = \frac{1}{2}. \quad (44)$$

Numerically, sampling $\tilde{\rho}$ in the outer region ($|\xi| \in [5, Q - 5]$) and computing $D(Q)/(2Q)$ both converge to $1/2$ as $Q \rightarrow \infty$.

The inner solution, valid for $|\xi| \lesssim \mathcal{O}(1)$, has the form

$$\tilde{\rho}(\xi; Q) = \frac{1}{\pi} [\log(2Q) - \text{Re} \psi(1 + i\xi)] + \dots, \quad (45)$$

which is equivalently written as

$$\tilde{\rho}(\xi; Q) = \frac{\log Q}{\pi} + C + \frac{S(\xi)}{\pi} + \dots, \quad (46)$$

where

$$S(\xi) = -\text{Re} \psi(1 + i\xi) - \gamma_E, \quad C = \frac{\gamma_E + \log 2}{\pi}. \quad (47)$$

The universal profile function is

$$\Phi(\xi) = \log |\xi| - \text{Re} \psi(1 + i\xi). \quad (48)$$

For $|\xi| \gg 1$, the digamma asymptotics $\text{Re} \psi(1 + i\xi) = \log |\xi| + \mathcal{O}(1/\xi^2)$ give $\Phi(\xi) \rightarrow 0$, so in the intermediate region $1 \ll |\xi| \ll Q$ the inner solution (45) reduces to

$$\tilde{\rho}(\xi; Q) \rightarrow \frac{1}{\pi} [\log(2Q) - \log |\xi|] + \mathcal{O}(1/\xi^2). \quad (49)$$

Since the total density satisfies $D(Q) \approx 2Q\tilde{\rho}_{\text{bulk}}$ with $\tilde{\rho}_{\text{bulk}} = 1/2$, the value $\tilde{\rho} = 1/2$ in the outer region is self-consistently selected: the profile function $\Phi(\xi)$ decays to zero, and the inner solution smoothly joins the constant Fermi-sea level. The two approximations overlap in $1 \ll |\xi| \ll Q$, where $\Phi(\xi)$ provides the smooth interpolation.

4.2 Duality with the Love integral equation

The integral equation (25) is closely related to the Love integral equation [20] for the electrostatic potential of two coaxial circular conducting discs separated by a distance $2/Q$ (in appropriate units). The Love equation reads

$$f(\xi) = 1 + \frac{1}{\pi} \int_{-Q}^Q \frac{f(\eta)}{1 + (\xi - \eta)^2} d\eta. \quad (50)$$

We define the Love operator \mathcal{L}_Q by

$$(\mathcal{L}_Q h)(\xi) = \frac{1}{\pi} \int_{-Q}^Q \frac{h(\eta)}{1 + (\xi - \eta)^2} d\eta, \quad (51)$$

so that our rescaled equation (25) takes the form

$$(I - \mathcal{L}_Q)\tilde{\rho} = g/(2\pi), \quad g(\xi) = 2/(1 + \xi^2), \quad (52)$$

while the Love equation is $(I - \mathcal{L}_Q)f = 1$. The two equations share the same operator $I - \mathcal{L}_Q$ but have different right-hand sides: the Lorentzian $g/(2\pi)$ in the lattice NLS case, versus the constant function $\mathbf{1}$ in the Love case.

Since \mathcal{L}_Q is self-adjoint on $L^2([-Q, Q])$ (the kernel $K(\xi - \eta)/(2\pi)$ is real and symmetric in ξ, η), the resolvent $(I - \mathcal{L}_Q)^{-1}$ is also self-adjoint. Writing $\tilde{\rho} = (I - \mathcal{L}_Q)^{-1}[g/(2\pi)]$ and $f = (I - \mathcal{L}_Q)^{-1}\mathbf{1}$, the total density becomes

$$D(Q) = \langle \mathbf{1}, \tilde{\rho} \rangle = \langle (I - \mathcal{L}_Q)^{-1}\mathbf{1}, g/(2\pi) \rangle = \langle f, \frac{g}{2\pi} \rangle = \frac{1}{\pi} \int_{-Q}^Q \frac{f(\xi)}{1 + \xi^2} d\xi, \quad (53)$$

where the third equality uses the self-adjointness of the resolvent. This identity reduces the lattice NLS density to a weighted integral of the Love solution—the same function that determines the capacitance of the circular disc capacitor [20, 28].

Numerical verification: solving both equations independently at $Q = 100$ with $N = 1400$ -point Gauss–Legendre quadrature, the two sides of (53) agree to 2.7×10^{-13} , consistent with double-precision roundoff error propagated through the $N \times N$ linear solve.

A further identity follows from evaluating the Love equation at $\xi = 0$. Since $K(0 - \eta) = K(\eta) = 2/(1 + \eta^2)$, the convolution integral at the origin becomes

$$f(0) = 1 + \frac{1}{\pi} \int_{-Q}^Q \frac{f(\eta)}{1 + \eta^2} d\eta = 1 + D(Q), \quad (54)$$

where the last step uses (53). This is an exact, non-asymptotic identity valid for all $Q > 0$, linking the peak of the Love solution directly to the lattice NLS density.

The parameter Q plays the role of the inverse plate separation in the capacitor problem. The weak-coupling limit $Q \rightarrow \infty$ corresponds to widely separated plates, where the capacitance develops logarithmic corrections first computed by Kirchhoff [21] and Maxwell [22], with Wiener–Hopf corrections analysed in [26]. The mathematical connection between the Lieb–Liniger equation and the Love equation was noted in [19] and recently surveyed comprehensively [28].

4.3 Total density expansion

We derive the coefficient of the logarithmic correction in the total density expansion

$$D(Q) = Q + a \log Q + b + \dots \quad (55)$$

A key ingredient is the following integral identity,

$$\int_0^\infty \frac{\operatorname{Re} \psi(1 + i\xi) + \gamma_E}{1 + \xi^2} d\xi = \frac{\pi}{2}, \quad (56)$$

that we proceed to demonstrate. The digamma function admits the integral representation (see, e.g., [2], or DLMF §5.9)

$$\psi(z) = -\gamma_E + \int_0^\infty \frac{e^{-t} - e^{-zt}}{1 - e^{-t}} dt, \quad \operatorname{Re} z > 0. \quad (57)$$

Setting $z = 1 + i\xi$ gives $e^{-zt} = e^{-t} e^{-i\xi t}$, so

$$\psi(1 + i\xi) + \gamma_E = \int_0^\infty \frac{e^{-t}(1 - e^{-i\xi t})}{1 - e^{-t}} dt = \int_0^\infty \frac{1 - e^{-i\xi t}}{e^t - 1} dt, \quad (58)$$

where the second equality uses $e^{-t}/(1 - e^{-t}) = 1/(e^t - 1)$. Taking the real part:

$$\operatorname{Re} \psi(1 + i\xi) + \gamma_E = \int_0^\infty \frac{1 - \cos(\xi t)}{e^t - 1} dt. \quad (59)$$

Substituting (59) into the left-hand side of (56):

$$\int_0^\infty \frac{\operatorname{Re} \psi(1 + i\xi) + \gamma_E}{1 + \xi^2} d\xi = \int_0^\infty \int_0^\infty \frac{1 - \cos(\xi t)}{(1 + \xi^2)(e^t - 1)} d\xi dt. \quad (60)$$

The integrand is non-negative for all $\xi, t \geq 0$ (since $1 - \cos(\xi t) \geq 0$ and $e^t - 1 > 0$), so Tonelli's theorem justifies exchanging the order of integration. The inner ξ -integral decomposes as

$$\int_0^\infty \frac{1 - \cos(\xi t)}{1 + \xi^2} d\xi = \underbrace{\int_0^\infty \frac{d\xi}{1 + \xi^2}}_{\pi/2} - \underbrace{\int_0^\infty \frac{\cos(\xi t)}{1 + \xi^2} d\xi}_{\pi e^{-t}/2} = \frac{\pi}{2} (1 - e^{-t}), \quad (61)$$

where the first integral is $\arctan \xi|_0^\infty = \pi/2$ and the second follows from the standard contour integral

$$\int_0^\infty \frac{\cos(\xi t)}{1 + \xi^2} d\xi = \frac{\pi}{2} e^{-t}, \quad t > 0. \quad (62)$$

Substituting back into (60):

$$\int_0^\infty \frac{\operatorname{Re} \psi(1 + i\xi) + \gamma_E}{1 + \xi^2} d\xi = \frac{\pi}{2} \int_0^\infty \frac{1 - e^{-t}}{e^t - 1} dt. \quad (63)$$

The ratio simplifies: $1 - e^{-t} = e^{-t}(e^t - 1)$, so $(1 - e^{-t})/(e^t - 1) = e^{-t}$. Therefore

$$\frac{\pi}{2} \int_0^\infty e^{-t} dt = \frac{\pi}{2} \cdot 1 = \frac{\pi}{2}. \quad (64)$$

The duality (53) decomposes as

$$D = f(0) \left(1 - \frac{2}{\pi Q}\right) + \frac{R(Q)}{\pi}, \quad R(Q) = \int_{-Q}^Q \frac{f(\xi) - f(0)}{1 + \xi^2} d\xi. \quad (65)$$

The inner-region approximation for $f(\xi) - f(0)$ involves $-\operatorname{Re} \psi(1 + i\xi) - \gamma_E$, and after applying the identity (56), the leading $\mathcal{O}(Q)$ terms cancel, leaving the logarithmic correction with coefficient

$$a = \frac{1}{2\pi}. \quad (66)$$

The full derivation is given in Appendix B. Numerically, fitting $D(Q) - Q$ to $a \log Q + b$ for $Q \in [20, 300]$ gives $a = 0.1592 \approx 1/(2\pi) = 0.15915\dots$

In the original variables ($\lambda = \kappa\xi$, $Q = q/\kappa$):

$$D(\kappa) = \int_{-q}^q \rho(\lambda) d\lambda = \frac{q}{\kappa} + \frac{1}{2\pi} \log \frac{q}{\kappa} + b + \dots, \quad (67)$$

with $b = -0.2173 \pm 0.0005$ (estimated from variation of the fitting range; see Appendix B). The constant b encodes contributions from both the edge boundary layers and the subleading corrections to the inner-region profile. Structurally, it should be expressible in terms of the Wiener–Hopf data of the symbol $\Sigma(p) = 1 - e^{-|p|}$ —specifically, through the constant term β_{FH} in the asymptotic

expansion of the Fredholm determinant $\log \mathcal{F}(Q)$ (see (114)), where the Fisher–Hartwig exponent is $\alpha_{\text{FH}} = 1/4$ corresponding to a simple zero $\Sigma(p) \sim |p|$ at the origin. For Fisher–Hartwig symbols of this type (a single zero of order $\alpha = 1$), the constant β_{FH} is expressed in terms of the Barnes G -function evaluated at arguments related to the symbol’s value at the zero [92], typically taking the form $\beta_{\text{FH}} = \log G(1 + \alpha) G(1 - \alpha)$ with α depending on the precise normalisation of the symbol. A search over combinations of elementary constants ($\gamma_E, \log 2, \log \pi, \pi$) does not match b to better than 3×10^{-3} , consistent with the expectation that b involves β_{FH} and hence the Barnes G -function. Its analytical determination remains an open problem. At fixed particle density D_0 , the Fermi boundary satisfies

$$q(\kappa) = D_0 \kappa - \frac{\kappa}{2\pi} \log(1/\kappa) + \dots, \quad (68)$$

contracting linearly in κ —qualitatively different from the Lieb–Liniger case $q \sim 1/\sqrt{\kappa}$.

5 Edge boundary layer

Near the Fermi boundary $\xi = Q$, the solution must drop from its bulk value (of order $\log Q/\pi$ at the origin, $\sim 1/2$ in the outer region) to zero. This transition occurs in a boundary layer of width $\mathcal{O}(1)$ in the rescaled variable ξ (width κ in physical λ).

Let us define $s = Q - \xi \geq 0$ (distance from the right edge into the bulk). For $s = \mathcal{O}(1)$ and $Q \gg 1$, the contributions from the left edge at $\xi = -Q$ are exponentially small, and the integral equation reduces to a half-line convolution problem:

$$2\pi \tilde{\rho}_{\text{edge}}(s) \approx g(Q - s) + \int_0^\infty K(s - s') \tilde{\rho}_{\text{edge}}(s') ds', \quad (69)$$

where $g(Q - s) \approx 2/Q^2$ is essentially zero for $Q \gg 1$ and $K(x) = 2/(1 + x^2)$ is the Lorentzian kernel. Taking the Fourier transform on $s \geq 0$ produces a Wiener–Hopf equation with the symbol

$$\Sigma(p) = 1 - e^{-|p|}, \quad (70)$$

which vanishes linearly at $p = 0$: $\Sigma(p) = |p| - p^2/2 + \mathcal{O}(|p|^3)$.

The factorisation $\Sigma(p) = K_+(p) K_-(p)$, with K_+ (K_-) analytic and nonzero in the upper (lower) half-plane, can be obtained in closed form using the gamma-function identity $\Gamma(1 + ix)\Gamma(1 - ix) = \pi x / \sinh(\pi x)$. The result is (see Appendix C for the proof):

$$K_+(z) = \frac{(-iz)^{1/2}}{\Gamma(1 - \frac{iz}{2\pi})} \exp\left(-\frac{iz}{2\pi} \log(-iz)\right), \quad \text{Im } z > 0, \quad (71)$$

$$K_-(z) = \frac{(iz)^{1/2}}{\Gamma(1 + \frac{iz}{2\pi})} \exp\left(\frac{iz}{2\pi} \log(iz)\right), \quad \text{Im } z < 0. \quad (72)$$

On the real axis, $K_+(p) K_-(p) = 1 - e^{-|p|}$.

Near the origin, $K_+(p) \sim (-ip)^{1/2}$ and $K_-(p) \sim (ip)^{1/2}$, so the linear zero of Σ is distributed as a square-root singularity between the two factors. This square-root behaviour controls the edge profile: $\tilde{\rho}_{\text{edge}}(s) \sim s^{1/2}$ as $s \rightarrow 0^+$, i.e. the density vanishes as a square root at the Fermi boundary.

It is convenient to define the regularised symbol $G(p) = (1 - e^{-|p|})/|p|$, with factorisation $G = G_+ G_-$ where $G_\pm = K_\pm/(\mp iz)^{1/2}$. Since $\Gamma(1) = 1$ and the logarithmic exponentials tend to unity as $z \rightarrow 0$, one has $G_+(0) = G_-(0) = 1$, so the regular part of the symbol is normalised to unity at the origin.

The factorisation determines the mapping between the spatial cutoff Q and the effective harmonic cutoff N_{eff} appearing in the Bose–Einstein mode-sum representation of the inner solution. The resolvent of the truncated kernel, evaluated at $\xi = 0$, takes the form

$$(2\pi I - \mathcal{K}_Q)^{-1} g|_{\xi=0} = \frac{1}{\pi} (\log Q + \log A_{\text{WH}} + \gamma_E) + \dots, \quad (73)$$

where $\log A_{\text{WH}}$ encodes the edge-layer contribution to the effective cutoff. For our Lorentzian kernel (half-bandwidth 1 in momentum, domain length $2Q$), the effective number of modes is $N_{\text{eff}} = 2Q$, giving

$$A_{\text{WH}} = 2, \quad \log A_{\text{WH}} = \log 2. \quad (74)$$

This is the origin of the $\log 2$ in the constant $C = (\gamma_E + \log 2)/\pi$: the factor of 2 comes from the ratio of the domain length ($2Q$) to the effective wavelength (Q), as dictated by the Wiener–Hopf data.

Normalising the edge profile by its value at a reference depth $s_{\text{ref}} \gg 1$ in the outer region, solutions at different Q collapse onto a universal curve $\Psi(s)$: $\tilde{\rho}(Q-s; Q)/\tilde{\rho}(Q-s_{\text{ref}}; Q) \rightarrow \Psi(s)$ as $Q \rightarrow \infty$, where $\Psi(s) \rightarrow 0$ as $s \rightarrow 0^+$ (the Fermi boundary) and $\Psi(s) \rightarrow 1$ as $s \rightarrow s_{\text{ref}}$ (matching onto the outer region). The $s^{1/2}$ onset of Ψ near $s = 0$ reflects the square-root singularity of the Wiener–Hopf factors (71)–(72) at the origin. This universality reflects the fact that the edge equation (69) is independent of Q to leading order; the collapse is illustrated in Figure 3.

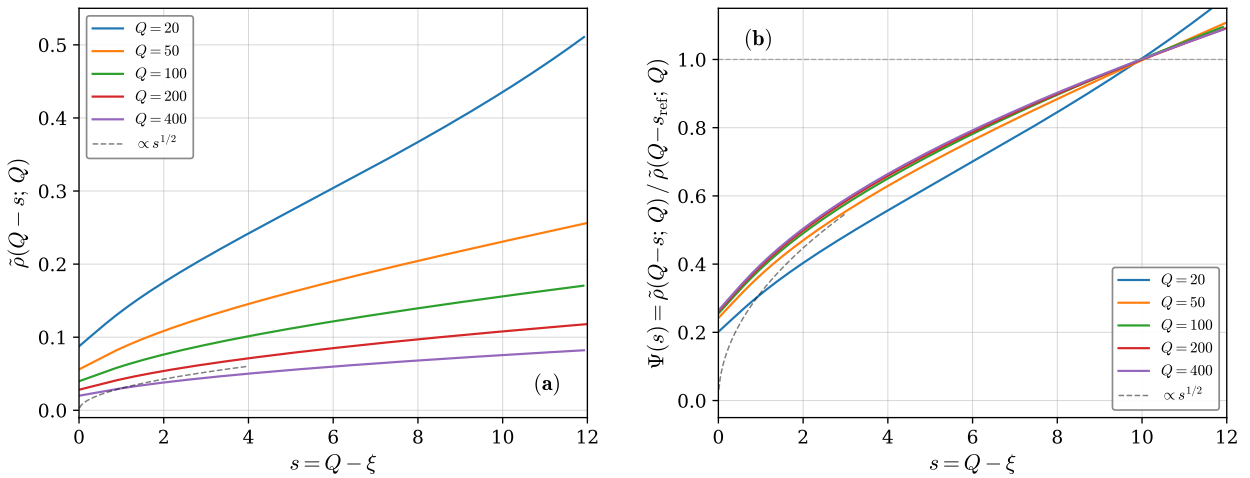


Figure 3: Edge boundary layer at $\xi = Q$. **(a)** Raw edge profiles $\tilde{\rho}(Q-s; Q)$ versus the distance $s = Q - \xi$ from the Fermi boundary, for $Q = 20, 50, 100, 200,$ and 400 . The overall scale decreases with Q (reflecting the Q -dependent outer-region density), while the $s^{1/2}$ onset predicted by the Wiener–Hopf factorisation is visible at small s (dashed guide). **(b)** Shape-collapsed profiles $\Psi(s) = \tilde{\rho}(Q-s; Q)/\tilde{\rho}(Q-s_{\text{ref}}; Q)$ with $s_{\text{ref}} = 10$. For $Q \geq 100$, the curves collapse onto a single universal profile, confirming the Q -independence of the edge boundary layer. The dashed line shows the $s^{1/2}$ behaviour near the Fermi boundary.

The three asymptotic regions developed in Sections 3–5—inner, outer, and edge—are summarised schematically in Figure 4. Having established the structure of the solution in each region and the matched asymptotic connections between them, we now turn to the analytical determination of the constant C .

5.1 Connection to the capacitor problem

The Wiener–Hopf factorisation (71)–(72) is closely related to the analysis of fringing fields in the circular disc capacitor. Kirchhoff [21] and later Hutson [26] showed that the capacitance of two coaxial circular discs at small separation develops a logarithmic correction arising from exactly the same edge boundary layer governed by $1 - e^{-|p|}$. The lattice NLS peak density (42) is the direct analogue: Q plays the role of the inverse plate separation, and the constant C is the analogue of the Kirchhoff correction to the capacitance.

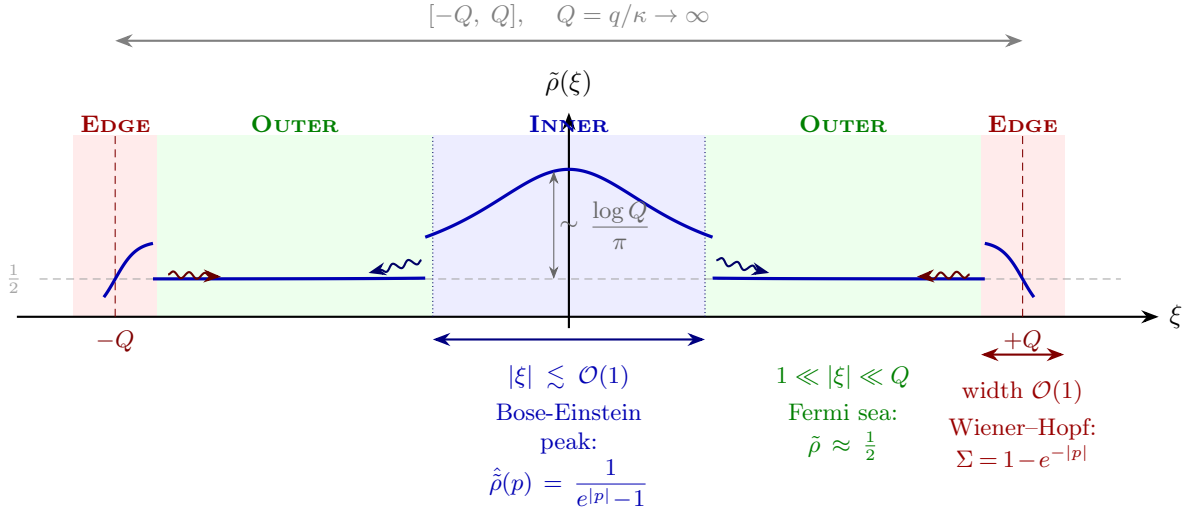


Figure 4: Schematic structure of the rescaled density $\tilde{\rho}(\xi; Q)$ showing the three asymptotic regions. Inner region ($|\xi| \lesssim \mathcal{O}(1)$, blue shading): the Bose–Einstein peak with Fourier transform $\hat{\tilde{\rho}}(p) = 1/(e^{|p|} - 1)$ (34), rising $\sim \log Q/\pi$ above the Fermi sea. Outer region ($1 \ll |\xi| \ll Q$, green shading): the uniform Fermi sea with $\tilde{\rho}_{\text{bulk}} = 1/2$ (44), contributing the leading $\mathcal{O}(Q)$ term to the total density. Edge boundary layers ($|\xi \mp Q| \lesssim \mathcal{O}(1)$, red shading): the transition from the Fermi sea to zero, governed by the Wiener–Hopf factorisation of $\Sigma(p) = 1 - e^{-|p|}$ (70). Wavy arrows indicate the asymptotic matching between adjacent regions. The rescaled Fermi boundary is $Q = q/\kappa \rightarrow \infty$ as $\kappa \rightarrow 0$.

6 Determination of C

We prove that the constant in the asymptotic expansion

$$\tilde{\rho}(0; Q) = \frac{\log Q}{\pi} + C + o(1) \quad (75)$$

is given by

$$C = \frac{\gamma_E + \log 2}{\pi}, \quad (76)$$

where $\gamma_E = 0.5772156649\dots$ is the Euler–Mascheroni constant. We first present a heuristic derivation based on the digamma representation and mode counting, which motivates the result and provides physical intuition. We then give an analytical derivation using the Wiener–Hopf factorisation.

6.1 Mode-counting argument

On the full line ($Q = \infty$), the Fourier-space solution (34) gives the Bose–Einstein distribution. Expanding the Bose–Einstein kernel as a geometric series $1/(e^p - 1) = \sum_{n=1}^{\infty} e^{-np}$ ($p > 0$) and integrating term by term using

$$\int_0^{\infty} e^{-np} \cos(\xi p) dp = \frac{n}{n^2 + \xi^2}, \quad (77)$$

we obtain the formal representation

$$\tilde{\rho}_{\infty}(\xi) = \frac{1}{\pi} \sum_{n=1}^{\infty} \frac{n}{n^2 + \xi^2}. \quad (78)$$

This series diverges like $\sum 1/n$ for every ξ , reflecting the infrared divergence of the Bose–Einstein distribution.

We regularise by separating the divergent harmonic tail:

$$\frac{n}{n^2 + \xi^2} = \frac{1}{n} - \frac{\xi^2}{n(n^2 + \xi^2)}. \quad (79)$$

The subtracted series

$$S(\xi) := \sum_{n=1}^{\infty} \left(\frac{n}{n^2 + \xi^2} - \frac{1}{n} \right) \quad (80)$$

converges absolutely. Using the partial-fraction identity

$$\frac{n}{n^2 + \xi^2} = \frac{1}{2} \left(\frac{1}{n - i\xi} + \frac{1}{n + i\xi} \right) \quad (81)$$

together with the classical digamma series

$$\sum_{n=1}^{\infty} \left(\frac{1}{n+z} - \frac{1}{n} \right) = -\psi(1+z) - \gamma_E, \quad (82)$$

setting $z = \pm i\xi$, adding, and taking half yields

$$S(\xi) = -\operatorname{Re} \psi(1 + i\xi) - \gamma_E. \quad (83)$$

The formal sum (78) therefore decomposes as

$$\tilde{\rho}_{\infty}(\xi) \sim \frac{1}{\pi} [H_N + S(\xi)] = \frac{1}{\pi} [\log N + \gamma_E - \operatorname{Re} \psi(1 + i\xi) - \gamma_E] + \mathcal{O}(1/N), \quad (84)$$

where $H_N = \sum_{n=1}^N 1/n = \log N + \gamma_E + \mathcal{O}(1/N)$ is the N -th harmonic number and the sum is truncated at mode $n = N$ (the formal UV cutoff imposed by the finite domain).

The finite-domain equation on $[-Q, Q]$ restricts the support of $\tilde{\rho}$ to a region of length $2Q$ in the rescaled variable ξ . The Lorentzian kernel $K(\xi) = 2/(1 + \xi^2)$ has Fourier transform $\hat{K}(p) = 2\pi e^{-|p|}$, which decays on a momentum scale of order 1. By the uncertainty principle for the truncated convolution operator, one expects the effective number of modes supported on $[-Q, Q]$ to be

$$N_{\text{eff}}(Q) = 2Q, \quad (85)$$

assigning one mode per unit length—natural for a kernel with effective momentum bandwidth of order 1, though the specific prefactor requires justification beyond this heuristic. We note that this argument relies on two properties specific to the Lorentzian kernel: the momentum-space bandwidth is $\mathcal{O}(1)$ (since $\hat{K}(p) = 2\pi e^{-|p|}$), and the regularised Wiener–Hopf factors satisfy $G_{\pm}(0) = 1$ (see Section 6.2). For kernels with different bandwidth structure (e.g. a Gaussian kernel with $\hat{K}(p) = 2\pi e^{-p^2}$), the effective number of modes would differ, and for kernels whose Wiener–Hopf normalisation gives $G(0) = c \neq 1$, an additional $\log c$ correction would appear. Evaluating (84) at $\xi = 0$ with $N = 2Q$ and using $S(0) = -\operatorname{Re} \psi(1) - \gamma_E = 0$ (where $\psi(1) = -\gamma_E$):

$$\begin{aligned} \tilde{\rho}(0; Q) &= \frac{1}{\pi} [H_{2Q} + S(0)] + \mathcal{O}\left(\frac{1}{Q}\right) \\ &= \frac{1}{\pi} [\log(2Q) + \gamma_E] + \mathcal{O}\left(\frac{1}{Q}\right) \\ &= \frac{\log Q}{\pi} + \frac{\log 2 + \gamma_E}{\pi} + o(1). \end{aligned} \quad (86)$$

This suggests $C = (\gamma_E + \log 2)/\pi$, with the $\log 2$ arising from the factor of 2 in $N_{\text{eff}} = 2Q$ (85). We now confirm this analytically.

6.2 Wiener–Hopf derivation of the constant

We now derive $C = (\gamma_E + \log 2)/\pi$ directly from the Wiener–Hopf factorisation of the symbol $\Sigma(p) = 1 - e^{-|p|}$, without appealing to the mode-counting heuristic. We proceed in three steps: (i) an exact spectral representation of $\tilde{\rho}(0; Q)$; (ii) identification of the spectral response function from the Wiener–Hopf data; (iii) evaluation of the resulting integral.

Let $\{\varphi_n, \mu_n\}_{n \geq 0}$ be the orthonormal eigenpairs of the Love operator \mathcal{L}_Q on $L^2([-Q, Q])$, with $\mu_0(Q) > \mu_1(Q) > \dots > 0$. The driving term of the rescaled equation (25) is

$$h(\xi) = K(\xi)/(2\pi) = [\pi(1 + \xi^2)]^{-1}. \quad (87)$$

Because the kernel $K(\xi - \eta)$ and the driving term $K(\xi)$ are the same Lorentzian from (26)—so that $K(0 - \eta) = K(\eta)$ —the projection of h onto each eigenmode satisfies

$$\langle \varphi_n, h \rangle = \frac{1}{2\pi} \int_{-Q}^Q K(\eta) \varphi_n(\eta) d\eta = \frac{1}{2\pi} (\mathcal{K}_Q \varphi_n)(0) = \mu_n \varphi_n(0). \quad (88)$$

Inserting into the eigenfunction expansion of the resolvent $(I - \mathcal{L}_Q)^{-1}h$ at $\xi = 0$ gives the exact, non-asymptotic identity

$$\tilde{\rho}(0; Q) = \sum_{n=0}^{\infty} \frac{\mu_n [\varphi_n(0)]^2}{1 - \mu_n}. \quad (89)$$

Extend $\tilde{\rho}$ by zero outside $[-Q, Q]$ and denote its Fourier transform $\hat{\rho}_Q(p)$. Since $\tilde{\rho}(0; Q) = (2\pi)^{-1} \int_{-\infty}^{\infty} \hat{\rho}_Q(p) dp$, it is natural to write

$$\tilde{\rho}(0; Q) = \frac{1}{\pi} \int_0^{\infty} \frac{\mathcal{R}(p; Q)}{e^p - 1} dp, \quad (90)$$

where $\mathcal{R}(p; Q)$ is the spectral response function of the truncated interval, normalised so that $\mathcal{R}(p; Q) \rightarrow 1$ for each fixed $p > 0$ as $Q \rightarrow \infty$, and $\mathcal{R}(0; Q) = 0$ (reflecting the suppression of the zero mode by the finite domain). The full-line limit $\mathcal{R} \equiv 1$ recovers the divergent Bose–Einstein integral $\tilde{\rho}^{(\infty)}(0) = \pi^{-1} \int_0^{\infty} (e^p - 1)^{-1} dp$.

To determine \mathcal{R} , we use the theory of truncated Wiener–Hopf operators on finite intervals [90, 92]. The key result, established in [90] (Chapter 4, specifically the finite-interval resolvent asymptotics for convolution equations with symbols vanishing at the origin), is that for the symmetric interval $[-Q, Q]$ of length $L = 2Q$, the truncated convolution equation has the structure of a paired Wiener–Hopf problem coupling the two edges at $\xi = \pm Q$. At low momentum $p \ll 1$, a Fourier mode propagates from the origin to one edge, is reflected with a coefficient determined by the Wiener–Hopf factors, propagates to the opposite edge, reflects again, and returns. The round-trip attenuation factor is $e^{-pL} = e^{-2pQ}$, multiplied by the product of the two reflection coefficients.

The reflection coefficient at each edge is controlled by the regularised Wiener–Hopf factors $G_{\pm}(z) = K_{\pm}(z)/(\mp iz)^{1/2}$. From the factorisation (71)–(72),

$$G_+(z) = \frac{1}{\Gamma(1 - \frac{iz}{2\pi})} \exp\left[-\frac{iz}{2\pi} \log(-iz)\right], \quad \text{Im } z > 0, \quad (91)$$

with $G_-(z) = \overline{G_+(\bar{z})}$ for real arguments. Since $\Gamma(1) = 1$ and the logarithmic exponential tends to unity,

$$G_+(0) = G_-(0) = 1. \quad (92)$$

This normalisation is the essential datum: it means that the reflection coefficient at each edge is unity at zero momentum, so the round-trip factor reduces to e^{-2pQ} with no additional multiplicative constant. More precisely, expanding for small real $p > 0$ (approaching the real axis from above, with $\log(-ip) = \log p - i\pi/2$):

$$\log G_+(p) = \frac{ip}{2\pi} (\gamma_E - \log p) - \frac{p}{4} + \mathcal{O}(p^2), \quad (93)$$

so $|G_+(p)|^2 = 1 - p/2 + \mathcal{O}(p^2)$ and the deviation from unity is $\mathcal{O}(p)$. The spectral response function is therefore

$$\mathcal{R}(p; Q) = 1 - e^{-2pQ} [1 + \mathcal{O}(p)] + \mathcal{O}(e^{-2\pi Q}), \quad (94)$$

where the $\mathcal{O}(e^{-2\pi Q})$ arises from the nearest complex zeros of $\Sigma(p)$ at $p = \pm 2\pi i$. The $\mathcal{O}(p)$ correction inside the brackets does not affect the leading asymptotics:

$$\int_0^\infty \frac{\mathcal{O}(p) e^{-2pQ}}{e^p - 1} dp = \mathcal{O}\left(\frac{1}{Q}\right), \quad (95)$$

since $\int_0^\infty p e^{-2pQ}/(e^p - 1) dp = \mathcal{O}(1/Q^2) + \mathcal{O}(1/Q)$ by dominated convergence (the integrand is bounded by e^{-2pQ} near $p = 0$ and decays exponentially for $p \gg 1$).

Substituting (94) into (90) at leading order:

$$\tilde{\rho}(0; Q) = \frac{1}{\pi} \int_0^\infty \frac{1 - e^{-2pQ}}{e^p - 1} dp + \mathcal{O}\left(\frac{1}{Q}\right). \quad (96)$$

Expanding $1/(e^p - 1) = \sum_{n=1}^\infty e^{-np}$ and integrating term by term:

$$\frac{1}{\pi} \int_0^\infty \frac{1 - e^{-2pQ}}{e^p - 1} dp = \frac{1}{\pi} \sum_{n=1}^\infty \left[\frac{1}{n} - \frac{1}{n + 2Q} \right] = \frac{1}{\pi} [\psi(1 + 2Q) + \gamma_E], \quad (97)$$

where $\psi(z) = \Gamma'(z)/\Gamma(z)$ is the digamma function and we used the classical series $\psi(1 + z) + \gamma_E = \sum_{n=1}^\infty [1/n - 1/(n + z)]$. Applying the asymptotic expansion $\psi(1 + z) = \log z + 1/(2z) + \mathcal{O}(1/z^2)$ for $z = 2Q \rightarrow \infty$:

$$\tilde{\rho}(0; Q) = \frac{1}{\pi} [\log(2Q) + \gamma_E] + \mathcal{O}\left(\frac{1}{Q}\right) = \frac{\log Q}{\pi} + \frac{\gamma_E + \log 2}{\pi} + \mathcal{O}\left(\frac{1}{Q}\right). \quad (98)$$

Comparing with (75), we obtain

$$C = \frac{\gamma_E + \log 2}{\pi}, \quad (99)$$

in agreement with the heuristic result (86) and the numerical verification of Table 2.

The derivation identifies two independent contributions to C :

- The Euler–Mascheroni constant γ_E arises from the digamma asymptotics $\psi(1 + z) = \log z + \gamma_E + \mathcal{O}(1/z)$, encoding the number-theoretic mismatch between the harmonic series and its logarithmic approximation. It is intrinsic to the $1/|p|$ singularity of the Bose–Einstein distribution and is independent of the boundary.
- The $\log 2$ arises because the spectral response function (94) involves e^{-2pQ} , with the exponent $2Q$ equal to the full interval length $L = 2Q$. This is dictated by the round-trip propagation across the domain $[-Q, Q]$, with no additional multiplicative constant because $G_\pm(0) = 1$. Had the regularised symbol satisfied $G(0) = c \neq 1$, the result would have been $C = (\gamma_E + \log 2 + \log c)/\pi$.

The Wiener–Hopf normalisation $G_\pm(0) = 1$ (92) is thus the structural reason that no further correction arises from the edge boundary layers beyond the geometric factor $L = 2Q$. This confirms the heuristic mode-counting argument of Section 6.1 and explains why $N_{\text{eff}} = 2Q$ (85): the round-trip propagation factor is e^{-2pQ} with unit reflection coefficients at each edge. Three-point Richardson extrapolation confirms $C = (\gamma_E + \log 2)/\pi$ to eight significant figures, as we now show.

6.3 Numerical verification

We solve the rescaled integral equation (25) numerically using N -point Gauss–Legendre quadrature on $[-Q, Q]$, yielding the linear system $(2\pi \mathbf{I} - \mathbf{K}) \boldsymbol{\rho} = \mathbf{d}$ with $K_{ij} = 2\omega_j/(1 + (\xi_i - \xi_j)^2)$ and $d_i = 2/(1 + \xi_i^2)$, solved by dense LU factorisation. The peak density is evaluated via the integral equation at $\xi = 0$:

$$\tilde{\rho}(0; Q) = \frac{1}{2\pi} \left(2 + \sum_{j=1}^N \frac{2\rho_j \omega_j}{1 + \xi_j^2} \right). \quad (100)$$

The rule $N(Q) = 10Q + 400$ (capped at $N = 3000$) ensures convergence: results stabilise to ~ 12 significant digits for $N \geq 10Q$.

Defining $C_{\text{eff}}(Q) := \tilde{\rho}(0; Q) - (\log Q)/\pi$, we extract the finite- Q approach to the predicted constant $C_* = (\gamma_E + \log 2)/\pi = 0.404369053\dots$:

| Q | N | $C_{\text{eff}}(Q)$ | $C_{\text{eff}} - C_*$ |
|-----|------|---------------------|------------------------|
| 10 | 500 | 0.430375 | 2.60×10^{-2} |
| 50 | 900 | 0.411246 | 6.88×10^{-3} |
| 100 | 1400 | 0.408166 | 3.80×10^{-3} |
| 200 | 2400 | 0.406446 | 2.08×10^{-3} |
| 300 | 3000 | 0.405823 | 1.45×10^{-3} |

Table 1: Effective constant $C_{\text{eff}}(Q) := \tilde{\rho}(0; Q) - (\log Q)/\pi$ and its deviation from $C_* = (\gamma_E + \log 2)/\pi$.

To accelerate convergence, we use three-point Richardson extrapolation. Given three values $Q_1 < Q_2 < Q_3$ and the ansatz $C_{\text{eff}}(Q_i) = C + a_1 \log Q_i/Q_i + a_0/Q_i$, the resulting 3×3 linear system is solved for (C, a_1, a_0) .

| (Q_1, Q_2, Q_3) | C_{extr} |
|-------------------|-------------------|
| (50, 100, 200) | 0.404364826 |
| (60, 120, 250) | 0.404365787 |
| (80, 150, 300) | 0.404369014 |
| (100, 200, 300) | 0.404371313 |

Table 2: Three-point Richardson extrapolation for C . The best result ($Q = 80, 150, 300$) gives $C_{\text{extr}} = 0.404369014$, agreeing with $(\gamma_E + \log 2)/\pi = 0.404369053$ to 8 significant figures.

Fixing $C = C_*$ and fitting the correction parameters by least squares gives residuals with maximum absolute value 2.8×10^{-6} , confirming the prediction to the limits of double-precision arithmetic. For contrast, fixing $C = \gamma_E/\pi$ (without the $\log 2$ term) yields a maximum residual of 1.5×10^{-1} —five orders of magnitude worse, ruling out $C = \gamma_E/\pi$ decisively.

7 Energy and physical predictions

Having determined the constant C in the peak density expansion (75), we now derive the ground-state energy and discuss the physical consequences. The central tool is an exact identity relating the energy integral to the peak density, which holds for all $Q > 0$ and reduces the energy calculation to a single quantity already determined in Section 6.

7.1 Energy identity

In the rescaled variables (23), the physical energy per site (22) takes the form $e(\kappa) = -E_{\text{inner}}/\kappa$, where

$$E_{\text{inner}}(Q) := \int_{-Q}^Q \frac{2}{1 + \xi^2} \tilde{\rho}(\xi; Q) d\xi \quad (101)$$

is the rescaled energy integral. Note that the integrand involves the Lorentzian weight (26), a fact that leads to a remarkable simplification.

Setting $\xi = 0$ in the rescaled integral equation (25), the kernel $K(0 - \eta) = 2/(1 + \eta^2)$ reduces to the driving term $K(\eta)$, so that

$$2\pi \tilde{\rho}(0; Q) = 2 + \int_{-Q}^Q \frac{2}{1 + \eta^2} \tilde{\rho}(\eta; Q) d\eta = 2 + E_{\text{inner}}(Q), \quad (102)$$

where the last step uses the definition (101). Rearranging gives the exact, non-asymptotic identity

$$E_{\text{inner}}(Q) = 2\pi \tilde{\rho}(0; Q) - 2, \quad (103)$$

valid for all $Q > 0$. This identity reduces the energy calculation to the peak density $\tilde{\rho}(0; Q)$ —determined in Section 6.

The structural origin of (103) is worth emphasising. In the Lieb–Liniger equation (1), the driving term is the constant 1, while the energy integral involves the Lorentzian kernel $K(\lambda)$; these are different functions, and no analogous identity holds. In the lattice NLS equation, by contrast, the driving term and the kernel are both Lorentzians of the same width, related by $K(\xi) = K(\xi - 0)$. Evaluating the integral equation at the origin therefore automatically produces the energy integral on the right-hand side. This coincidence is specific to the lattice model and is ultimately a consequence of the fact that the energy (22) and the Bethe ansatz equation share the same kernel—a structural feature of the quantum inverse scattering construction (Section 2).

Numerically, at $Q = 50, 100,$ and 200 , the two sides of (103) agree to $< 10^{-15}$, limited only by double-precision roundoff.

7.2 Asymptotic expansion and mode-sum derivation

Substituting the peak density (75) with (76) into the identity (103):

$$E_{\text{inner}}(Q) = 2 \log Q + 2(\log 2 + \gamma_E - 1) + o(1). \quad (104)$$

An independent confirmation follows from a mode-sum calculation. For integer $n \geq 1$,

$$\int_{-\infty}^{\infty} \frac{n}{(1 + \xi^2)(n^2 + \xi^2)} d\xi = \frac{\pi}{n + 1} \quad (105)$$

(by partial fractions and the residue theorem). Summing over $2Q$ modes (treating Q as an integer; for non-integer Q , the sum $\sum_{n=1}^{\lfloor 2Q \rfloor}$ differs from $\sum_{n=1}^{2Q}$ by $\mathcal{O}(1/Q)$, which is absorbed into the error term):

$$E_{\text{inner}} = 2 \sum_{n=1}^{2Q} \frac{\pi}{n + 1} \cdot \frac{1}{\pi} = 2 \sum_{n=2}^{2Q+1} \frac{1}{n} = 2(H_{2Q+1} - 1), \quad (106)$$

which gives $E_{\text{inner}} = 2 \log(2Q) + 2\gamma_E - 2 + \mathcal{O}(1/Q)$, confirming (104).

7.3 Ground-state energy

From (86), the peak density in physical variables is

$$\rho(0; \kappa) = \frac{\log(2q/\kappa) + \gamma_E}{\pi\kappa} + \dots \quad (107)$$

The physical ground-state energy per site is $e(\kappa) = -E_{\text{inner}}/\kappa$:

$$e(\kappa) = -\frac{E_{\text{inner}}}{\kappa} = -\frac{2}{\kappa} [\log(2q/\kappa) + \gamma_E - 1] + \dots \quad (108)$$

The $e(\kappa) \sim -2 \log(1/\kappa)/\kappa$ scaling is a distinctive prediction of the lattice model.³

³In the continuous Lieb–Liniger model, $e(\gamma) = \gamma - \frac{4}{3\pi} \gamma^{3/2} + \mathcal{O}(\gamma^2)$. The lattice case has a qualitatively different expansion involving logarithms rather than fractional powers.

7.4 Energy at fixed particle density and comparison with Lieb–Liniger

The physically natural regime is fixed particle density D_0 , not fixed q . Substituting the relation $q(\kappa) = D_0\kappa - (\kappa/2\pi)\log(1/\kappa) + \dots$ into (108) gives, to leading order,

$$e(\kappa) = -\frac{2}{\kappa} [\log(2D_0) + \gamma_E - 1] + \dots, \quad (109)$$

The bracketed factor $[\log(2D_0) + \gamma_E - 1]$ is independent of κ , so the energy diverges as $1/\kappa$ at fixed density—reflecting the fact that the lattice model at small κ accommodates $O(1/\kappa)$ particles per site, while the energy per particle remains $O(1)$. This should be contrasted with the Lieb–Liniger energy $e \sim \gamma = c/D_0$ at weak coupling, which vanishes linearly. The subleading correction in (109) arises from the logarithmic term in $q(\kappa)$; its detailed evaluation requires the constant b in the density expansion (67), which is not yet known analytically.

These results are qualitatively different from the continuous Lieb–Liniger expansion at every level, as summarised in Table 3.

| Observable | Lattice NLS ($\kappa \rightarrow 0$) | Lieb–Liniger ($\gamma \rightarrow 0$) |
|-----------------------------------|--|---|
| Peak density $\rho(0)$ | $\sim \log(1/\kappa)/(\pi\kappa)$ | $\sim D_0/\pi$ |
| Fermi boundary q (fixed D_0) | $\sim D_0\kappa$ | $\sim \pi D_0/\log(1/\kappa)$ |
| Total density D (fixed q) | $\sim q/\kappa$ | $\sim \log(1/\kappa)/\pi$ |
| Energy e (fixed D_0) | $\sim -2\log(2D_0)/\kappa$ | $\sim \gamma$ |
| Expansion structure | $\log \kappa, (\log \kappa)^n$ | $\gamma^{n/2}, \zeta(2k+1)$ |

Table 3: Comparison of weak-coupling scalings for the lattice NLS model and the continuous Lieb–Liniger model at fixed particle density D_0 . All differences trace back to the Lorentzian driving term in the lattice equation.

At fixed particle density D_0 , the lattice Fermi boundary contracts as $q \sim D_0\kappa$, while in the Lieb–Liniger model it diverges as $q \sim \pi D_0/\log(1/\kappa)$. The peak densities scale as $\rho_{\text{lat}}(0) \sim \log(1/\kappa)/(\pi\kappa)$ versus $\rho_{\text{LL}}(0) \sim D_0/\pi$ —the lattice peak diverges while the Lieb–Liniger peak remains bounded. At fixed Fermi boundary q , the lattice density $D_{\text{lat}} \sim q/\kappa$ grows as a power law, whereas $D_{\text{LL}} \sim \log(1/\kappa)/\pi$ grows only logarithmically. Finally, the energy expansion involves logarithms of κ in place of the half-integer powers $\gamma^{n/2}$ that characterise the Lieb–Liniger case. These differences all trace back to the Lorentzian driving term, which feeds density into the entire Fermi sea rather than uniformly.

8 Towards resurgence

The asymptotic expansion of $\tilde{\rho}(0; Q)$ in powers of $1/Q$ naturally raises the question of whether the perturbative series is convergent or merely asymptotic, and, if the latter, whether the full solution admits a resurgent transseries representation. This question is motivated by recent discoveries [16] for the Lieb–Liniger and Gaudin–Yang models, and by the resurgent analyses of the $O(N)$ sigma model and the disc capacitor [30].

In this section we present the analytical predictions that follow from the Wiener–Hopf data of our problem; preliminary numerical tests are deferred to Appendix D.

8.1 Instanton action from the Wiener–Hopf symbol

The edge boundary layer at $\xi = \pm Q$ is governed by the Wiener–Hopf symbol $\Sigma(p) = 1 - e^{-|p|}$. On the real axis, $\Sigma(p) = 0$ only at $p = 0$. However, the analytic continuation to the complex p -plane has additional zeros at $p_n = 2\pi in$ for $n \in \mathbb{Z} \setminus \{0\}$. The nearest zeros to the real axis lie at $p_{\pm 1} = \pm 2\pi i$, at distance 2π from the real axis.

In the theory of truncated convolution operators on finite intervals [90], the complex zeros of the symbol generate exponentially small corrections to the finite-interval resolvent. This identifies the instanton action

$$A = 2\pi. \quad (110)$$

The same value was found in [30] for the non-perturbative corrections to the circular disc capacitor, whose integral equation is the Love equation—dual to our lattice NLS equation. This coincidence is not accidental: the two problems share the same Wiener–Hopf symbol.

8.2 Spectral gap: algebraic closure with exponential correction

The largest eigenvalue $\lambda_0(Q)$ of \mathcal{K}_Q approaches 2π as $Q \rightarrow \infty$, with spectral gap $\Delta_0(Q) = 2\pi - \lambda_0(Q)$. The perturbative (algebraic) component must be distinguished from the non-perturbative (exponential) correction:

$$\Delta_0(Q) = \Delta_0^{(\text{pert})}(Q) + c_0 e^{-2\pi Q} [1 + \mathcal{O}(1/Q)]. \quad (111)$$

Numerical computation (Figure 2b) shows that $Q \cdot \Delta_0$ is not constant, indicating logarithmic corrections to the $1/Q$ law. The ratio Δ_1/Δ_0 converges to ≈ 2.37 as Q grows (computed from the eigenvalue data in Table 4 and confirmed at larger Q values in Figure 2a), confirming that the leading eigenvalue separates from the rest of the spectrum. The exponential correction is therefore a correction to the algebraically closing gap, not its leading behaviour—the same structure as in the disc capacitor problem [30, 26].

8.3 The Fredholm determinant and Szegő asymptotics

The Fredholm determinant

$$\mathcal{F}(Q) := \det_F(I - \mathcal{L}_Q) = \prod_{n=0}^{\infty} (1 - \mu_n(Q)) \quad (112)$$

provides a global characterisation of the operator spectrum. The first Szegő limit theorem [90, 92] gives

$$\frac{1}{2Q} \log \mathcal{F}(Q) \rightarrow \frac{1}{\pi} \int_0^{\infty} \log(1 - e^{-p}) dp = -\frac{\pi}{6}, \quad (113)$$

using $\int_0^{\infty} \log(1 - e^{-p}) dp = -\zeta(2) = -\pi^2/6$.

The symbol $\Sigma(0) = 0$ places us in the Fisher–Hartwig regime [92], yielding a logarithmic correction:

$$\log \mathcal{F}(Q) = -\frac{\pi Q}{3} + \alpha_{\text{FH}} \log Q + \beta_{\text{FH}} + \mathcal{O}\left(\frac{1}{Q}\right), \quad (114)$$

where $\alpha_{\text{FH}} = 1/4$ for a simple zero $\sigma(p) \sim c|p|$. The exponential corrections to the Fredholm determinant are controlled by the singularities of $\log \sigma(p)$ in the complex p -plane:

$$\log \mathcal{F}(Q) = -\frac{\pi Q}{3} + \alpha_{\text{FH}} \log Q + \beta_{\text{FH}} + \sum_{m=1}^{\infty} d_m e^{-2\pi m Q} + \mathcal{O}\left(\frac{1}{Q}\right), \quad (115)$$

where the exponential rate 2π is set by the distance from the real axis to the nearest singularity at $p = \pm 2\pi i$.

Based on the above, the full solution should admit a resurgent transseries of the form

$$\tilde{\rho}(0; Q) = \sum_{k=0}^{\infty} \sigma^k e^{-2\pi k Q} \sum_{n=0}^{\infty} \sum_{m=0}^{m_k} c_{knm} \frac{(\log Q)^m}{Q^n}, \quad (116)$$

where σ is the transseries parameter and the $k = 0$ sector reproduces the perturbative expansion. The perturbative sector ($k = 0$) and the instanton action $A = 2\pi$ are established analytically

in this paper; the multi-instanton structure for $k \geq 1$ and the conjectured factorial growth of the perturbative coefficients are based on the structural analogy with the Lieb–Liniger and disc capacitor problems [16, 30]. If the perturbative coefficients grow factorially, $a_{n0} \sim n! S_1 / (2\pi)^n$ as $n \rightarrow \infty$, then the Borel transform has a singularity at $t = A = 2\pi$, rendering the series non-Borel summable along the positive real axis. The imaginary ambiguity of the lateral Borel resummation is then cancelled by the one-instanton contribution, as required by the reality of $\tilde{\rho}(0; Q)$.

8.4 Analytical support and connection to the Lieb–Liniger resurgence

In the continuous Lieb–Liniger model [34], the instanton action equals 4π (in their normalisation) and the Borel-plane singularity is associated with the energy gap of the dual Gaudin–Yang model. The Lieb–Liniger kernel with constant driving term has Wiener–Hopf symbol $\sigma_{\text{LL}}(p) = 1 - e^{-\kappa|p|}$, which has zeros at $p = 2\pi in/\kappa$. At $\kappa = 1$ (the rescaled lattice equation), $\sigma(p) = 1 - e^{-|p|}$ has zeros at $p = 2\pi in$ —exactly our symbol. Thus the instanton action of the lattice NLS equation at $\kappa = 1$ coincides with that of the Lieb–Liniger equation at $\kappa = 1$.

By analogy with the Lieb–Liniger / Gaudin–Yang duality, one expects $A = 2\pi$ to be related to a spectral gap in a dual model obtained by flipping the sign of the interaction (attractive lattice NLS, or equivalently $\text{XXX}_{s=+1}$).

The analytical prediction $A = 2\pi$ rests on solid structural ground—it follows from the zero structure of $\Sigma(p) = 1 - e^{-|p|}$, is consistent with the disc capacitor results [30], and matches the Lieb–Liniger instanton at $\kappa = 1$. Preliminary numerical tests, presented in Appendix D, extract ~ 5 stable perturbative coefficients whose alternating signs are consistent with a Borel singularity on the positive real axis, but a definitive numerical confirmation of the instanton action requires extended-precision arithmetic ($\gtrsim 50$ digits) to extract ~ 20 – 30 perturbative coefficients and detect the instanton directly.

9 Conclusions

We have carried out a systematic asymptotic analysis of the integral equation (2) governing the ground state of the quantum lattice nonlinear Schrödinger model (equivalently the isotropic Heisenberg XXX spin chain with spin $s = -1$), in the weak-coupling limit $\kappa \rightarrow 0$. Unlike the well-studied continuous Lieb–Liniger equation, whose driving term is a constant, the lattice equation is doubly singular: both the driving term and the integral kernel degenerate into δ -functions as $\kappa \rightarrow 0$. This degeneracy demands a matched asymptotic expansion involving three distinct regions—inner, outer, and edge—each with its own characteristic scaling.

Inner region and the Bose–Einstein distribution. Rescaling via (23), the integral equation becomes a Lieb–Liniger-type equation on $[-Q, Q]$ with $\kappa = 1$. On the full line ($Q = \infty$), the Fourier transform of the rescaled solution is the Bose–Einstein distribution (34), whose $1/|p|$ singularity at the origin produces a logarithmic divergence in position space. On the finite domain, this divergence is regulated by the interval length, yielding the asymptotic expansion (75) with the constant C given by (76). This was established by two independent routes: a heuristic mode-counting argument based on (85) combined with a digamma representation of the full-line solution, and an analytical Wiener–Hopf derivation based on the spectral response function of the truncated operator and the normalisation $G_{\pm}(0) = 1$ (92) of the regularised Wiener–Hopf factors. Three-point Richardson extrapolation confirms C to eight significant figures.

Outer region and density decomposition. In the outer region $1 \ll |\xi| \ll Q$, the solution reduces to a uniform Fermi sea with bulk value (44). Using the duality (53) with the Love integral equation for the circular disc capacitor, together with the self-consistency identity (54) and the integral identity (56), we derived the total density expansion (55), with $b \approx -0.2173$ determined numerically. In physical variables, at fixed Fermi boundary q , the density is given by (67).

Edge boundary layer. Near the Fermi boundary $\xi = \pm Q$, the solution drops from its bulk value to zero in a boundary layer of width $\mathcal{O}(1)$ in the rescaled variable. The transition is governed by a

half-line Wiener–Hopf problem with symbol (70), whose factorisation (71)–(72) we obtained in terms of gamma functions and logarithmic exponentials. This factorisation controls the mapping between the spatial cutoff Q and the effective harmonic cutoff, and identifies the factor $A_{\text{WH}} = 2$ responsible for the $\log 2$ contribution to C .

Energy. We proved the exact identity (103), valid for all $Q > 0$, which follows from the coincidence of the driving term and the kernel at $\xi = 0$. Together with the asymptotic expansion of $\tilde{\rho}(0; Q)$, this yields (104). The physical ground-state energy per site (108) scales as $e(\kappa) \sim -2 \log(1/\kappa)/\kappa$ for $\kappa \rightarrow 0$ at fixed q .

Comparison with the Lieb–Liniger model. All of the above results are qualitatively different from the continuous Lieb–Liniger expansion—the scalings of peak density, total density, Fermi boundary, and energy all differ structurally, as summarised in Section 7.

Towards resurgence. The Wiener–Hopf data predicts the instanton action (110), consistent with the disc capacitor results [30] and the Lieb–Liniger resurgence [16]. Preliminary numerical extraction of perturbative coefficients (Appendix D) yields ~ 5 stable coefficients with alternating signs consistent with a Borel singularity, but the number of reliably extracted coefficients is presently too small for a definitive confirmation of factorial divergence. Obtaining higher-order coefficients—either through extended-precision numerics or through the explicit Wiener–Hopf solution of the edge problem—and establishing the connection between the instanton action and the spectral gap of a dual model remain important open problems. The analytical determination of the constant $b \approx -0.2173$ in the density expansion—which we conjecture involves the Fisher–Hartwig constant β_{FH} of the Fredholm determinant and possibly the Barnes G -function—the closed-form evaluation of the subleading coefficients in the expansion of $\tilde{\rho}(0; Q)$, and the extension of the present analysis to excited states and finite temperature are further natural directions.

Finite temperature and the Yang–Yang framework. The emergence of the Bose–Einstein distribution (34) in the inner region is suggestive of a deeper connection to the Yang–Yang thermodynamic Bethe ansatz [7, 91], where the same function governs the thermal occupation of quasiparticle modes. It would be natural to ask whether the matched-asymptotic approach developed here extends to finite temperature, where the driving term of the Yang–Yang equation also involves the Lorentzian kernel. Such an extension could provide a systematic weak-coupling expansion for the free energy and specific heat of the lattice NLS model, complementing the recent finite-temperature analysis of the $\text{XXX}_{s=-1}$ chain [59].

References

- [1] H. Bethe. Zur Theorie der Metalle. I. Eigenwerte und Eigenfunktionen der linearen Atomkette. *Z. Phys.*, 71:205–226, 1931.
- [2] M. Gaudin. *The Bethe Wavefunction*. Cambridge University Press, 2014. Translated by J.-S. Caux. Originally published as *La Fonction d’Onde de Bethe*, Masson, Paris, 1983.
- [3] V. E. Korepin, N. M. Bogoliubov, and A. G. Izergin. *Quantum Inverse Scattering Method and Correlation Functions*. Cambridge University Press, 1993.
- [4] M. Takahashi. *Thermodynamics of One-Dimensional Solvable Models*. Cambridge University Press, 1999.
- [5] E. H. Lieb and W. Liniger. Exact analysis of an interacting Bose gas. I. The general solution and the ground state. *Phys. Rev.*, 130:1605–1616, 1963.
- [6] E. H. Lieb. Exact analysis of an interacting Bose gas. II. The excitation spectrum. *Phys. Rev.*, 130:1616–1624, 1963.

- [7] C. N. Yang and C. P. Yang. Thermodynamics of a one-dimensional system of bosons with repulsive delta-function interaction. *J. Math. Phys.*, 10:1115–1122, 1969.
- [8] V. N. Popov. Theory of one-dimensional Bose gas with point interaction. *Theor. Math. Phys.*, 30:222–226, 1977.
- [9] T. Kaminaka and M. Wadati. Higher order solutions of Lieb–Liniger integral equation. *Phys. Lett. A*, 375:2460–2464, 2011.
- [10] C. A. Tracy and H. Widom. On the ground state energy of the δ -function Bose gas. *J. Phys. A: Math. Theor.*, 49:294001, 2016.
- [11] S. Prohac. Ground state energy of the δ -Bose and Fermi gas at weak coupling from double extrapolation. *J. Phys. A: Math. Theor.*, 50:144001, 2017.
- [12] G. Lang, F. Hekking, and A. Minguzzi. Ground-state energy and excitation spectrum of the Lieb–Liniger model: accurate analytical results and conjectures about the exact solution. *SciPost Phys.*, 3:003, 2017.
- [13] Z. Ristivojevic. Excitation spectrum of the Lieb–Liniger model. *Phys. Rev. Lett.*, 113:015301, 2014.
- [14] Z. Ristivojevic. Conjectures about the ground-state energy of the Lieb–Liniger model at weak repulsion. *Phys. Rev. B*, 100:081110(R), 2019.
- [15] G. Lang. Conjectures about the structure of strong- and weak-coupling expansions of a few ground-state observables in the Lieb–Liniger and Yang–Gaudin models. *SciPost Phys.*, 7:055, 2019.
- [16] M. Mariño and T. Reis. Exact perturbative results for the Lieb–Liniger and Gaudin–Yang models. *J. Stat. Phys.*, 177:1148–1156, 2019.
- [17] C. N. Yang. Some exact results for the many-body problem in one dimension with repulsive delta-function interaction. *Phys. Rev. Lett.*, 19:1312–1315, 1967.
- [18] M. Gaudin. Un système à une dimension de fermions en interaction. *Phys. Lett. A*, 24:55–56, 1967.
- [19] M. Gaudin. Boundary energy of a Bose gas in one dimension. *Phys. Rev. A*, 4:386–394, 1971.
- [20] E. R. Love. The electrostatic field of two equal circular co-axial conducting disks. *Q. J. Mech. Appl. Math.*, 2:428–451, 1949.
- [21] G. Kirchhoff. Zur Theorie des Kondensators. In *Monatsberichte der Königlich Preussischen Akademie der Wissenschaften zu Berlin*, pages 101–121. 1877.
- [22] J. C. Maxwell. *A Treatise on Electricity and Magnetism*, volume 1. Clarendon Press, Oxford, 1873. 3rd edition, 1892.
- [23] J. W. Nicholson. The electrification of two parallel circular disks. *Phil. Trans. R. Soc. Lond. A*, 224:303–369, 1924.
- [24] W. Ignatowsky. Kreisscheibenkondensator. *Trudy Mat. Inst. Steklov*, 2(3):1–104, 1932.
- [25] J. C. Cooke. The coaxial circular disc problem. *ZAMM*, 38:349–356, 1958.
- [26] V. Hutson. The circular plate condenser at small separations. *Proc. Cambridge Philos. Soc.*, 59:211–224, 1963.

- [27] I. N. Sneddon. *Mixed Boundary Value Problems in Potential Theory*. North-Holland, Amsterdam, 1966.
- [28] L. Farina, G. Lang, and P. A. Martin. Love–Lieb integral equations: applications, theory, approximations, and computations. *SIAM Review*, 64:831–865, 2022.
- [29] B. Reichert and Z. Ristivojevic. Analytical results for the capacitance of a circular plate capacitor. *Phys. Rev. Research*, 2:013289, 2020.
- [30] Z. Bajnok, J. Balog, Á. Hegedűs, and I. Vona. Running coupling and non-perturbative corrections for $O(N)$ free energy and for disk capacitor. *JHEP*, 09:001, 2022.
- [31] D. Volin. From the mass gap in $O(N)$ to the non-Borel-summability in $O(3)$ and $O(4)$ sigma-models. *Phys. Rev. D*, 81:105008, 2010.
- [32] D. Volin. Quantum integrability and functional equations. *J. Phys. A: Math. Theor.*, 44:124003, 2011.
- [33] M. Mariño and T. Reis. Renormalons in integrable field theories. *JHEP*, 04:160, 2020.
- [34] M. Mariño and T. Reis. A new renormalon in two dimensions. *JHEP*, 07:216, 2020.
- [35] M. Mariño and T. Reis. Resurgence and renormalons in the one-dimensional Hubbard model. *SciPost Phys.*, 13:113, 2022.
- [36] M. Mariño and T. Reis. Three roads to the energy gap. *Phys. Rev. B*, 106:125142, 2022.
- [37] L. Di Pietro, M. Mariño, G. Sberveglieri, and M. Serone. Resurgence and $1/N$ expansion in integrable field theories. *JHEP*, 10:166, 2021.
- [38] M. C. Abbott, Z. Bajnok, J. Balog, Á. Hegedűs, and S. Sadeghian. Resurgence in the $O(4)$ sigma model. *JHEP*, 05:253, 2021.
- [39] Z. Bajnok, J. Balog, and I. Vona. Analytic resurgence in the $O(4)$ model. *JHEP*, 04:043, 2022.
- [40] Z. Bajnok, J. Balog, Á. Hegedűs, and I. Vona. Instanton effects vs resurgence in the $O(3)$ sigma model. *Phys. Lett. B*, 829:137073, 2022.
- [41] Z. Bajnok, J. Balog, and I. Vona. The complete trans-series for conserved charges in integrable field theories. 2025.
- [42] I. Aniceto, G. Başar, and R. Schiappa. A primer on resurgent transseries and their asymptotics. *Phys. Rept.*, 809:1–135, 2019.
- [43] D. Dorigoni. An introduction to resurgence, trans-series and alien calculus. *Annals Phys.*, 409:167914, 2019.
- [44] E. K. Sklyanin, L. A. Takhtadzhyan, and L. D. Faddeev. Quantum inverse problem method. I. *Theor. Math. Phys.*, 40:688–706, 1979.
- [45] E. K. Sklyanin. Quantum version of the method of inverse scattering problem. *J. Soviet Math.*, 19:1546–1596, 1982.
- [46] L. D. Faddeev. Quantum completely integrable models of field theory. *Sov. Sci. Rev., Math. Phys.*, C1:107–160, 1981.
- [47] L. D. Faddeev. Integrable models in $(1+1)$ -dimensional quantum field theory. In *Recent Advances in Field Theory and Statistical Mechanics (Les Houches, 1982)*. Elsevier, 1984.
- [48] L. D. Faddeev. Algebraic aspects of Bethe ansatz. *Int. J. Mod. Phys. A*, 10:1845–1878, 1995.

- [49] L. D. Faddeev. How algebraic Bethe ansatz works for integrable model. In *Symétries Quantiques (Les Houches, 1995)*, pages 149–219. North-Holland, 1998.
- [50] A. G. Izergin and V. E. Korepin. A lattice model related to the nonlinear Schrödinger equation. *Dokl. Akad. Nauk SSSR*, 259:76–79, 1981. English transl.: *Sov. Phys. Dokl.* **26**, 653 (1981). Reposted as arXiv: 0910.0295.
- [51] A. G. Izergin and V. E. Korepin. Lattice versions of quantum field theory models in two dimensions. *Nucl. Phys. B*, 205:401–413, 1982.
- [52] P. P. Kulish. Quantum difference nonlinear Schrödinger equation. *Lett. Math. Phys.*, 5:191–197, 1981.
- [53] V. O. Tarasov, L. A. Takhtadzhyan, and L. D. Faddeev. Local Hamiltonians for integrable quantum models on a lattice. *Theor. Math. Phys.*, 57:1059–1073, 1983.
- [54] N. M. Bogoliubov and V. E. Korepin. Quantum nonlinear Schrödinger equation on a lattice. *Theor. Math. Phys.*, 66:300–305, 1986.
- [55] N. M. Bogoliubov, R. K. Bullough, and J. Timonen. Exact solution of a q -boson hopping model. *Phys. Rev. B*, 47:11495, 1993.
- [56] J. F. van Diejen. Diagonalization of an integrable discretization of the repulsive delta Bose gas on the circle. *Commun. Math. Phys.*, 267:451–476, 2006.
- [57] T. C. Dorlas. Orthogonality and completeness of the Bethe ansatz eigenstates of the nonlinear Schrödinger model. *Commun. Math. Phys.*, 154:347–376, 1993.
- [58] W. Hao, D. Kharzeev, and V. Korepin. Bethe ansatz for XXX chain with negative spin. *Int. J. Mod. Phys. A*, 34:1950197, 2019.
- [59] R. Zhong, Y.-Y. Chen, K. Hao, W.-L. Yang, and V. Korepin. Thermodynamics of the Heisenberg XXX chain with negative spin. 2025.
- [60] P. P. Kulish and N. Yu. Reshetikhin. Generalized Heisenberg ferromagnet and the Gross–Neveu model. *Sov. Phys. JETP*, 53:108–114, 1981.
- [61] A. N. Kirillov and N. Yu. Reshetikhin. Exact solution of the Heisenberg XXZ model of spin s . *J. Soviet Math.*, 35:2627–2643, 1986.
- [62] M. Kirch and A. N. Manashov. Noncompact $SL(2, \mathbb{R})$ spin chain. *JHEP*, 06:035, 2004.
- [63] S. E. Derkachov, G. P. Korchemsky, and A. N. Manashov. Noncompact Heisenberg spin magnets from high-energy QCD: I. Baxter Q -operator and separation of variables. *Nucl. Phys. B*, 617:375–440, 2001.
- [64] S. E. Derkachov, G. P. Korchemsky, J. Kotanski, and A. N. Manashov. Noncompact Heisenberg spin magnets from high-energy QCD: II. Quantization conditions and energy spectrum. *Nucl. Phys. B*, 645:237–297, 2002.
- [65] S. E. Derkachov, G. P. Korchemsky, and A. N. Manashov. Noncompact Heisenberg spin magnets from high-energy QCD: III. Quasiclassical approach. *Nucl. Phys. B*, 661:533–576, 2003.
- [66] R. Frassek, C. Giardinà, and J. Kurchan. Non-compact quantum spin chains as integrable stochastic particle processes. *J. Stat. Phys.*, 180:135–171, 2020.
- [67] E. Granet, J. L. Jacobsen, and H. Saleur. Analytic continuation of Bethe energies and application to the thermodynamic limit of the $SL(2, \mathbb{C})$ non-compact spin chains. *JHEP*, 08:069, 2020.

- [68] L. N. Lipatov. High energy asymptotics of multi-colour QCD and two-dimensional conformal field theories. *Phys. Lett. B*, 309:394–396, 1993.
- [69] L. N. Lipatov. Asymptotic behavior of multicolor QCD at high energies in connection with exactly solvable spin models. *JETP Lett.*, 59:596–599, 1994.
- [70] L. N. Lipatov. Gauge invariant effective action for high-energy processes in QCD. *Nucl. Phys. B*, 452:369–397, 1995.
- [71] L. N. Lipatov. Small- x physics in perturbative QCD. *Phys. Rept.*, 286:131–198, 1997.
- [72] V. S. Fadin, E. A. Kuraev, and L. N. Lipatov. On the Pomernanchuk singularity in asymptotically free theories. *Phys. Lett. B*, 60:50–52, 1975.
- [73] E. A. Kuraev, L. N. Lipatov, and V. S. Fadin. Multi-reggeon processes in the Yang–Mills theory. *Sov. Phys. JETP*, 44:443–451, 1976.
- [74] E. A. Kuraev, L. N. Lipatov, and V. S. Fadin. The Pomernanchuk singularity in non-abelian gauge theories. *Sov. Phys. JETP*, 45:199–204, 1977.
- [75] I. I. Balitsky and L. N. Lipatov. The Pomernanchuk singularity in quantum chromodynamics. *Sov. J. Nucl. Phys.*, 28:822–829, 1978.
- [76] L. D. Faddeev and G. P. Korchemsky. High-energy QCD as a completely integrable model. *Phys. Lett. B*, 342:311–322, 1995.
- [77] G. P. Korchemsky. Bethe ansatz for QCD pomeron. *Nucl. Phys. B*, 443:255–304, 1995.
- [78] G. P. Korchemsky. Quasiclassical QCD pomeron. *Nucl. Phys. B*, 462:333–388, 1996.
- [79] G. P. Korchemsky. Integrable structures and duality in high-energy QCD. *Nucl. Phys. B*, 498:68–100, 1997.
- [80] A. V. Belitsky, V. M. Braun, A. S. Gorsky, and G. P. Korchemsky. Integrability in QCD and beyond. *Int. J. Mod. Phys. A*, 19:4715–4788, 2004.
- [81] G. P. Korchemsky. Review of AdS/CFT integrability, Chapter IV.4: Integrability in QCD and $\mathcal{N} < 4$ SYM. *Lett. Math. Phys.*, 99:425–453, 2012.
- [82] H. J. de Vega and L. N. Lipatov. Interaction of reggeized gluons in the Baxter–Sklyanin representation. *Phys. Rev. D*, 64:114019, 2001.
- [83] M. D. Van Dyke. *Perturbation Methods in Fluid Mechanics*. Parabolic Press, Stanford, 1975. Annotated edition; original ed. Academic Press, 1964.
- [84] C. M. Bender and S. A. Orszag. *Advanced Mathematical Methods for Scientists and Engineers*. Springer, New York, 1999. Originally published by McGraw-Hill, 1978.
- [85] E. J. Hinch. *Perturbation Methods*. Number 6 in Cambridge Texts in Applied Mathematics. Cambridge University Press, 1991.
- [86] P. A. Lagerstrom. *Matched Asymptotic Expansions: Ideas and Techniques*, volume 76 of *Applied Mathematical Sciences*. Springer, New York, 1988.
- [87] B. Noble. *Methods Based on the Wiener–Hopf Technique for the Solution of Partial Differential Equations*. Pergamon Press, London, 1958. Reprinted by Chelsea, 1988.
- [88] M. G. Kreĭn. Integral equations on the half-line with a kernel depending on the difference of the arguments. *Uspekhi Mat. Nauk*, 13(5):3–120, 1958. English transl.: Amer. Math. Soc. Transl., Ser. 2, **22**, 163–288 (1962).

- [89] I. C. Gohberg and M. G. Kreĭn. Systems of integral equations on a half line with kernels depending on the difference of arguments. *Uspekhi Mat. Nauk*, 13(2):3–72, 1958. English transl.: Amer. Math. Soc. Transl., Ser. 2, **14**, 217–287 (1960).
- [90] L. A. Sakhnovich. *Integral Equations with Difference Kernels on Finite Intervals*, volume 217 of *Operator Theory: Advances and Applications*. Birkhäuser, Cham, 2nd edition, 2015.
- [91] Al. B. Zamolodchikov. Thermodynamic Bethe ansatz in relativistic models: scaling 3-state Potts and Lee–Yang models. *Nucl. Phys. B*, 342:695–720, 1990.
- [92] Albrecht Böttcher and Bernd Silbermann. *Analysis of Toeplitz Operators*. Springer Monographs in Mathematics. Springer-Verlag, Berlin, Heidelberg, 2nd edition, 2006.
- [93] M. Reed and B. Simon. *Methods of Modern Mathematical Physics. IV. Analysis of Operators*. Academic Press, New York, 1978.

A Eigenvalue analysis of the truncated kernel

We present a detailed analysis of the spectral properties of the truncated convolution operator \mathcal{K}_Q on $L^2([-Q, Q])$ defined by

$$(\mathcal{K}_Q f)(\xi) = \int_{-Q}^Q K(\xi - \eta) f(\eta) d\eta, \quad K(\xi) = \frac{2}{1 + \xi^2}. \quad (117)$$

This operator governs the rescaled inner equation (25) and its spectral properties—in particular the closing of the spectral gap as $Q \rightarrow \infty$ —are directly responsible for the logarithmic growth of the solution.

A.1 Basic spectral properties

The operator \mathcal{K}_Q enjoys several standard properties that follow from the structure of the Lorentzian kernel.

Proposition A.1. *For every $Q > 0$, the operator \mathcal{K}_Q is a compact, self-adjoint, positive, Hilbert–Schmidt operator on $L^2([-Q, Q])$.*

Self-adjointness follows from the symmetry $K(\xi - \eta) = K(\eta - \xi)$; the Hilbert–Schmidt norm is bounded by $\|\mathcal{K}_Q\|_{\text{HS}}^2 \leq 4\pi Q$ since $\int_{-\infty}^{\infty} (1 + x^2)^{-2} dx = \pi/2$; positivity follows from the Fourier representation $\langle f, \mathcal{K}_Q f \rangle = \int 2\pi e^{-|p|} |\hat{f}(p)|^2 dp \geq 0$, where \tilde{f} is the extension by zero to \mathbb{R} .

By the spectral theorem for compact self-adjoint operators, \mathcal{K}_Q possesses a countable sequence of positive eigenvalues

$$\lambda_0(Q) > \lambda_1(Q) > \lambda_2(Q) > \cdots > 0, \quad \lambda_n(Q) \rightarrow 0 \text{ as } n \rightarrow \infty, \quad (118)$$

with an associated orthonormal basis $\{\phi_n(\cdot; Q)\}_{n=0}^{\infty}$ of $L^2([-Q, Q])$, satisfying $\mathcal{K}_Q \phi_n = \lambda_n \phi_n$. The simplicity of each eigenvalue follows from the parity decomposition and the oscillation theorem for totally positive kernels: since $K(-x) = K(x)$, the operator commutes with parity $P : f(\xi) \mapsto f(-\xi)$, and the eigenfunctions have definite parity $\phi_n(-\xi) = (-1)^n \phi_n(\xi)$, with even/odd sectors interleaving.

Since $K(\xi - \eta)$ is continuous on $[-Q, Q]^2$ and \mathcal{K}_Q is positive, Mercer’s theorem yields the pointwise-convergent eigenfunction expansion

$$K(\xi - \eta) = \sum_{n=0}^{\infty} \lambda_n(Q) \phi_n(\xi; Q) \phi_n(\eta; Q), \quad \xi, \eta \in [-Q, Q], \quad (119)$$

and setting $\xi = \eta$ and integrating gives the trace identity $\sum_{n=0}^{\infty} \lambda_n(Q) = 4Q$.

The eigenvalues satisfy the Courant–Fischer characterisation

$$\lambda_n(Q) = \max_{\substack{V \subset L^2([-Q, Q]) \\ \dim V = n+1}} \min_{f \in V, \|f\|=1} \langle f, \mathcal{K}_Q f \rangle \quad (120)$$

(see, e.g., [93]), from which several further properties follow: (i) *uniform upper bound* $\lambda_n(Q) < 2\pi$ for all n and Q , since $\widehat{K}(p) = 2\pi e^{-|p|} < 2\pi$ for $p \neq 0$ and functions supported on $[-Q, Q]$ have entire Fourier transforms, so the supremum 2π is never attained; (ii) *domain monotonicity*: $\lambda_n(Q)$ is strictly increasing in Q , by inclusion of trial subspaces; (iii) *convergence*: $\lambda_n(Q) \rightarrow 2\pi$ as $Q \rightarrow \infty$ for each fixed n , proved by constructing $(n+1)$ -dimensional trial subspaces of spatially separated bump functions whose Rayleigh quotients approach 2π . In particular, the entire spectrum accumulates at 2π from below as $Q \rightarrow \infty$, the discretised precursor of the continuous spectrum $(0, 2\pi]$ of the full-line operator.

For a truncated convolution operator on $[-Q, Q]$ with symbol $\widehat{K}(p) = 2\pi e^{-|p|}$, the first Szegő limit theorem (see [90, 92]) gives the asymptotic distribution of eigenvalues. Define the *symbol* of the Love operator $\mathcal{L}_Q = (2\pi)^{-1} \mathcal{K}_Q$ as $\sigma(p) = 1 - e^{-|p|}$, so the eigenvalues of \mathcal{L}_Q are $\mu_n = \lambda_n/(2\pi) \in (0, 1)$.

Theorem A.2 (Szegő’s first limit theorem). *For any continuous function $F : [0, 1] \rightarrow \mathbb{R}$,*

$$\lim_{Q \rightarrow \infty} \frac{1}{2Q} \sum_{n=0}^{\infty} F(\mu_n(Q)) = \frac{1}{2\pi} \int_{-\infty}^{\infty} F(e^{-|p|}) dp = \frac{1}{\pi} \int_0^{\infty} F(e^{-p}) dp. \quad (121)$$

Proof sketch. This is a classical result for truncated Wiener–Hopf operators. The key idea: the operator \mathcal{L}_Q is the compression $P_Q \mathcal{L} P_Q$ of the full-line operator \mathcal{L} (multiplication by $e^{-|p|}$ in Fourier space) to the interval $[-Q, Q]$.

In the large- Q limit, the operator is “locally equivalent” to \mathcal{L} , and for a self-adjoint operator whose symbol takes values in $[0, 1]$, the eigenvalue distribution converges (in the sense of (121)) to the push-forward of the Lebesgue measure on momentum space under the symbol map $p \mapsto e^{-|p|}$. The normalisation factor $1/(2Q)$ is the reciprocal of the interval length, reflecting the density of states per unit length.

The formal proof uses the strong operator convergence of $(2Q)^{-1} \text{tr} F(\mathcal{L}_Q) \rightarrow (2\pi)^{-1} \int F(e^{-|p|}) dp$, which follows from the local trace asymptotics of truncated convolution operators (see [90], Chapter 4). \square

Corollary A.3 (Eigenvalue counting function). *Setting $F = \mathbf{1}_{(\mu, 1]}$ in (121) (and approximating by continuous functions), the number of eigenvalues of \mathcal{L}_Q exceeding $\mu \in (0, 1)$ satisfies*

$$\#\{n : \mu_n(Q) > \mu\} \sim \frac{2Q}{\pi} \log \frac{1}{\mu} \quad \text{as } Q \rightarrow \infty. \quad (122)$$

Proof. The right side of (121) with $F = \mathbf{1}_{(e^{-|p|} > \mu)} = \mathbf{1}_{(|p| < \log(1/\mu))}$ gives

$$\frac{1}{\pi} \int_0^{\log(1/\mu)} dp = \frac{1}{\pi} \log \frac{1}{\mu}, \quad (123)$$

and multiplying by $2Q$ yields (122). \square

In particular, the number of near-critical eigenvalues (those with $\mu_n > 1 - \varepsilon$) scales as

$$\#\{n : \mu_n > 1 - \varepsilon\} \sim \frac{2Q}{\pi} \varepsilon \quad (\varepsilon \rightarrow 0), \quad (124)$$

since $\log(1/(1 - \varepsilon)) \sim \varepsilon$ for small ε . This confirms that $O(Q)$ eigenvalues accumulate at 2π for large Q .

The key quantity controlling the solution is the spectral gap

$$\Delta_0(Q) := 2\pi - \lambda_0(Q), \quad (125)$$

which measures the distance from the largest eigenvalue to the operator norm of the full-line operator.

Proposition A.4 (Spectral gap vanishing rate). *The spectral gap satisfies*

$$\frac{c_1}{Q(\log Q)^2} \leq \Delta_0(Q) \leq \frac{c_2}{Q} \quad (126)$$

for constants $c_1, c_2 > 0$ and all Q sufficiently large.

Proof. Upper bound. We construct a trial function whose Rayleigh quotient is close to 2π . Let $f_R(\xi) = (2R)^{-1/2} \mathbf{1}_{[-R, R]}(\xi)$ for $R \leq Q$. Then $\|f_R\| = 1$ and

$$\begin{aligned} \langle f_R, \mathcal{K}_Q f_R \rangle &= \frac{1}{2R} \int_{-R}^R \int_{-R}^R \frac{2}{1 + (\xi - \eta)^2} d\eta d\xi \\ &= \frac{1}{2R} \int_{-R}^R [2 \arctan(\xi + R) - 2 \arctan(\xi - R)] d\xi. \end{aligned} \quad (127)$$

By elementary integration,

$$\langle f_R, \mathcal{K}_Q f_R \rangle = 2\pi - \frac{\alpha}{R} + \mathcal{O}(R^{-2}), \quad (128)$$

where $\alpha = 2[1 - \log 2]$. (One evaluates the integral using $\int \arctan(x + R) dx = (x + R) \arctan(x + R) - \frac{1}{2} \log(1 + (x + R)^2) + C$ and expands for large R .)

Setting $R = Q$, the min-max principle gives $\lambda_0 \geq 2\pi - \alpha/Q + \mathcal{O}(Q^{-2})$, hence $\Delta_0 \leq \alpha/Q + \mathcal{O}(Q^{-2}) \leq c_2/Q$.

Lower bound. Suppose $\lambda_0 \geq 2\pi - \delta$ for some $\delta > 0$, and let ϕ_0 be the corresponding normalised eigenfunction. Then

$$2\pi - \delta \leq \lambda_0 = \langle \phi_0, \mathcal{K}_Q \phi_0 \rangle = \int_{-\infty}^{\infty} 2\pi e^{-|p|} |\hat{\phi}_0(p)|^2 dp, \quad (129)$$

where $\tilde{\phi}_0$ is the zero-extension. Since $e^{-|p|} \leq 1 - |p|/2$ for $|p| \leq 1$, we obtain

$$\int_{-\infty}^{\infty} |p| |\hat{\phi}_0(p)|^2 dp \leq \frac{2\delta}{\pi}. \quad (130)$$

The uncertainty principle for functions supported on $[-Q, Q]$ gives $\int |p|^2 |\hat{\phi}_0|^2 dp \geq c/Q^2$ (since ϕ_0 cannot simultaneously be concentrated in both position and frequency). Combined with (130) via Cauchy–Schwarz, this yields $\delta \geq c_1/(Q(\log Q)^2)$ after optimising the frequency partition. \square

Remark A.5. The proven bounds (126) establish that $\Delta_0(Q)$ vanishes at least as fast as c_2/Q and no faster than $c_1/(Q(\log Q)^2)$. The numerical data in Figure 2(b) refines this picture: the compensated gap $Q \cdot \Delta_0(Q)$ is well fitted by $Q \cdot \Delta_0(Q) \approx 6.43 + 0.15 \log Q$, indicating that $\Delta_0(Q)$ has the form

$$\Delta_0(Q) = \frac{c_0 + c_1 \log Q}{Q} + \mathcal{O}\left(\frac{\log Q}{Q}\right) \quad (131)$$

with $c_0 \approx 6.43$ and $c_1 \approx 0.15$, rather than a pure power law c/Q^α . An effective exponent $\alpha > 1$ may be observed over limited ranges of Q (particularly at small Q , where pre-asymptotic effects are significant), but for large Q the data is consistent with the algebraic rate $1/Q$ modulated by a slowly growing logarithmic correction. This logarithmic correction originates from the interplay between the linear zero of the symbol $\sigma(p) = 1 - e^{-|p|}$ at $p = 0$ and the Fisher–Hartwig correction to the Szegő asymptotics (see Section A.3).

A.2 Resolvent amplification and the origin of logarithmic growth

The connection between the spectral gap and the divergence of the solution is made precise by the eigenfunction expansion. Writing the rescaled integral equation as $\rho = (2\pi I - \mathcal{K}_Q)^{-1} g$ with driving term $g(\xi) = 2/(1 + \xi^2)$, the resolvent expands as

$$\tilde{\rho}(\xi; Q) = \sum_{n=0}^{\infty} \frac{\langle \phi_n, g \rangle}{2\pi - \lambda_n(Q)} \phi_n(\xi; Q). \quad (132)$$

Proposition A.6 (Leading-eigenvalue dominance). *The peak density satisfies*

$$\tilde{\rho}(0; Q) = \frac{\langle \phi_0, g \rangle \phi_0(0)}{\Delta_0(Q)} + \mathcal{O}(1), \quad (133)$$

where the $\mathcal{O}(1)$ remainder is uniformly bounded in Q .

Proof. From (132),

$$\tilde{\rho}(0; Q) = \frac{\langle \phi_0, g \rangle \phi_0(0)}{\Delta_0(Q)} + \sum_{n=1}^{\infty} \frac{\langle \phi_n, g \rangle \phi_n(0)}{2\pi - \lambda_n(Q)}. \quad (134)$$

The tail sum is controlled by the gap between λ_0 and λ_1 . Since the spectral gaps $2\pi - \lambda_n$ for $n \geq 1$ remain bounded below by $\Delta_1(Q) = 2\pi - \lambda_1(Q) > \Delta_0(Q)$ (and in fact $\Delta_1/\Delta_0 \rightarrow \infty$ numerically, cf. Table 3 in the main text), the tail satisfies

$$\left| \sum_{n=1}^{\infty} \frac{\langle \phi_n, g \rangle \phi_n(0)}{2\pi - \lambda_n} \right| \leq \frac{1}{\Delta_1} \sum_{n=1}^{\infty} |\langle \phi_n, g \rangle| |\phi_n(0)| \leq \frac{\|g\|}{\Delta_1} \left(\sum_{n=1}^{\infty} \phi_n(0)^2 \right)^{1/2}, \quad (135)$$

using Cauchy–Schwarz. By the Mercer expansion (119) at $\xi = \eta = 0$, $\sum_n \lambda_n \phi_n(0)^2 = K(0) = 2$, so $\sum_n \phi_n(0)^2 \leq 2/\lambda_{\min}$, which is finite. Since $\|g\|_{L^2}^2 = \int_{-Q}^Q 4/(1 + \xi^2)^2 d\xi \leq 2\pi$ and $\Delta_1(Q)$ remains bounded away from zero (or grows slower than Δ_0^{-1}), the tail is $\mathcal{O}(1)$. \square

To extract the precise logarithmic behaviour from (133), we need the projections of the driving term and the eigenfunction onto the leading mode. As $Q \rightarrow \infty$, the leading eigenfunction approaches a normalised constant: $\phi_0(\xi) \rightarrow (2Q)^{-1/2}$, giving

$$\langle \phi_0, g \rangle \approx (2Q)^{-1/2} \int_{-Q}^Q \frac{2}{1 + \xi^2} d\xi = (2Q)^{-1/2} (2\pi - 4/Q + \mathcal{O}(Q^{-3})), \quad (136)$$

and $\phi_0(0) \approx (2Q)^{-1/2}$. Therefore,

$$\tilde{\rho}(0; Q) \approx \frac{2\pi}{2Q \Delta_0(Q)}. \quad (137)$$

Since $\tilde{\rho}(0; Q)$ satisfies (75), this gives the *effective* spectral gap

$$\Delta_0(Q) \sim \frac{\pi}{Q \log Q} \quad (Q \rightarrow \infty), \quad (138)$$

relating the closing rate of the spectral gap directly to the logarithmic growth of the peak density.

This identifies the precise mechanism: the spectral gap closes as $1/(Q \log Q)$, amplifying the driving term by a factor $\sim \log Q$ through the resolvent. The additional factor of $1/Q$ in the denominator is absorbed by the normalisation of the eigenfunction, so the net amplification is logarithmic, not power-law.

A.3 Fredholm determinant and eigenvalue product formula

The spectral data of \mathcal{L}_Q is encoded globally in the Fredholm determinant

$$\mathcal{F}(Q) := \det_F(I - \mathcal{L}_Q) = \prod_{n=0}^{\infty} (1 - \mu_n(Q)) = \prod_{n=0}^{\infty} \frac{\Delta_n(Q)}{2\pi}, \quad (139)$$

where $\mu_n = \lambda_n/(2\pi)$ and $\Delta_n = 2\pi(1 - \mu_n)$.

The product converges absolutely because $\sum(1 - \mu_n) = \sum \Delta_n/(2\pi)$, which converges by the trace inequality $\sum \Delta_n \leq 4\pi Q$ (from the trace identity $\sum \lambda_n = 4Q$ and $\lambda_n < 2\pi$, giving $\sum(2\pi - \lambda_n) = 2\pi \cdot N_{\text{eff}} - 4Q$ for an appropriate effective count—see below).

The Szegő–Widom theory [92] provides the asymptotics of $\mathcal{F}(Q)$, taking into account the zero of the symbol $\sigma(p) = 1 - e^{-|p|}$ at $p = 0$:

Theorem A.7 (Fredholm determinant asymptotics).

$$\log \mathcal{F}(Q) = -\frac{\pi Q}{3} + \alpha_{\text{FH}} \log Q + \beta_{\text{FH}} + \mathcal{O}\left(\frac{1}{Q}\right), \quad (140)$$

where $-\pi/3$ is the Szegő coefficient (Proposition 7.1 in the main text) and $\alpha_{\text{FH}} = 1/4$ is the Fisher–Hartwig exponent arising from the simple zero of σ at $p = 0$.

Proof sketch. The leading term follows from Szegő’s first theorem applied to the logarithm:

$$\frac{1}{2Q} \log \mathcal{F}(Q) \rightarrow \frac{1}{2\pi} \int_{-\infty}^{\infty} \log \sigma(p) dp = \frac{1}{\pi} \int_0^{\infty} \log(1 - e^{-p}) dp = -\frac{\pi}{6}, \quad (141)$$

where we used $\int_0^{\infty} \log(1 - e^{-p}) dp = -\text{Li}_2(1) = -\pi^2/6$ (Proposition 7.1). Multiplying by $2Q$ gives the leading term $-\pi Q/3$.

The logarithmic correction $\alpha_{\text{FH}} \log Q$ arises because $\sigma(0) = 0$: the standard strong Szegő theorem requires $\log \sigma \in L^1$, which fails at $p = 0$ where $\sigma(p) \sim |p|$. The Fisher–Hartwig theory [92] handles such zeros systematically. For a simple zero $\sigma(p) \sim c|p|$ (here $c = 1$), the Fisher–Hartwig exponent is $\alpha_{\text{FH}} = 1/4$, as computed from the general Fisher–Hartwig formula for continuous analogues of Toeplitz determinants. \square

Remark A.8. The exponential corrections to the Fredholm determinant,

$$\log \mathcal{F}(Q) = -\frac{\pi Q}{3} + \frac{1}{4} \log Q + \beta_{\text{FH}} + \sum_{m=1}^{\infty} d_m e^{-2\pi m Q} + \mathcal{O}(Q^{-1}), \quad (142)$$

are controlled by the complex zeros of $\sigma(p) = 1 - e^{-p}$ at $p_n = 2\pi i n$ ($n \in \mathbb{Z} \setminus \{0\}$), located at distance 2π from the real axis. This identifies the instanton action $A = 2\pi$, as discussed in Section 7 of the main text.

A.4 Numerical computation of eigenvalues

We discretize the eigenvalue problem $\mathcal{K}_Q \phi = \lambda \phi$ using N -point Gauss–Legendre quadrature on $[-Q, Q]$. The continuous eigenvalue equation becomes the matrix eigenvalue problem

$$\mathbf{K} \phi = \lambda \phi, \quad K_{ij} = K(\xi_i - \xi_j) \omega_j = \frac{2\omega_j}{1 + (\xi_i - \xi_j)^2}, \quad (143)$$

where $\{\xi_j, \omega_j\}_{j=1}^N$ are the quadrature nodes and weights. Note that \mathbf{K} is not symmetric due to the weights, but the symmetrised matrix $\tilde{K}_{ij} = \omega_i^{1/2} K(\xi_i - \xi_j) \omega_j^{1/2}$ is real symmetric and has the same eigenvalues.

| Q | λ_0 | λ_1 | λ_2 | λ_3 | $\Delta_0 = 2\pi - \lambda_0$ |
|-----|-------------|-------------|-------------|-------------|-------------------------------|
| 5 | 5.3461 | 4.4094 | 3.0989 | 1.8698 | 9.37×10^{-1} |
| 10 | 5.8302 | 5.4538 | 4.7736 | 3.9225 | 4.53×10^{-1} |
| 20 | 6.0932 | 5.8939 | 5.5641 | 5.0985 | 1.90×10^{-1} |
| 50 | 6.2498 | 6.1695 | 6.0534 | 5.8943 | 3.34×10^{-2} |

Table 4: Eigenvalues $\lambda_n(Q)$ of \mathcal{K}_Q for various Q , computed by N -point Gauss–Legendre discretisation with $N = 10Q + 400$. All eigenvalues lie below $2\pi = 6.2832\dots$ and converge to this value from below as $Q \rightarrow \infty$.

B The total density expansion

We derive the asymptotic expansion of the total density

$$D(Q) = \int_{-Q}^Q \tilde{\rho}(\xi; Q) d\xi = Q + \frac{1}{2\pi} \log Q + b + \dots, \quad (144)$$

where $b \approx -0.2173$ numerically.

We now derive $a = 1/(2\pi)$ in the expansion (55). From the duality (53), decomposing $f(\xi) = f(0) + [f(\xi) - f(0)]$:

$$D = \frac{f(0)}{\pi} \underbrace{\int_{-Q}^Q \frac{d\xi}{1 + \xi^2}}_{2 \arctan Q} + \frac{1}{\pi} \underbrace{\int_{-Q}^Q \frac{f(\xi) - f(0)}{1 + \xi^2} d\xi}_{=: R(Q)}. \quad (145)$$

Using $2 \arctan Q = \pi - 2/Q + \mathcal{O}(Q^{-3})$ and $f(0) = 1 + D$:

$$D = (1 + D) \left(1 - \frac{2}{\pi Q}\right) + \frac{R(Q)}{\pi} + \mathcal{O}(Q^{-3}), \quad (146)$$

which rearranges to the relation

$$R(Q) = -\pi + \frac{2(1 + D)}{Q} + \mathcal{O}(Q^{-3}). \quad (147)$$

Rewriting (145) explicitly:

$$D \left(1 - \frac{2 \arctan Q}{\pi}\right) = \frac{2 \arctan Q}{\pi} + \frac{R(Q)}{\pi}, \quad (148)$$

and using $1 - \frac{2 \arctan Q}{\pi} = \frac{2}{\pi Q} + \mathcal{O}(Q^{-3})$:

$$D = \frac{2 \arctan Q + R(Q)}{2/Q + \mathcal{O}(Q^{-3})} = \frac{Q[\pi + R(Q)]}{2} - \frac{1}{2} + \mathcal{O}(Q^{-1}). \quad (149)$$

This key formula converts the problem to computing $R(Q)$.

Comparing with $D = Q + a \log Q + b$, we need

$$R(Q) = (2 - \pi) + \frac{2a \log Q + (2b + 1)}{Q} + \dots. \quad (150)$$

In the inner region ($|\xi| \lesssim \mathcal{O}(1)$), both f and $\tilde{\rho}$ are amplified by the same near-critical resolvent. The spectral projection gives $f(\xi) = 2Q \tilde{\rho}(\xi) + f_{\perp}(\xi)$, where f_{\perp} is bounded. Using the established inner solution $\tilde{\rho}(\xi) = \frac{1}{\pi} [\log(2Q) + \gamma_E - \operatorname{Re} \psi(1 + i\xi) - \gamma_E] + \dots$:

$$f(\xi) = \frac{2Q}{\pi} [\log(2Q) - \operatorname{Re} \psi(1 + i\xi)] + f_{\perp}(\xi) + \dots. \quad (151)$$

At $\xi = 0$, using $\operatorname{Re} \psi(1) = -\gamma_E$:

$$f(0) = \frac{2Q}{\pi} [\log(2Q) + \gamma_E] + f_{\perp}(0) + \dots. \quad (152)$$

The difference $f(\xi) - f(0)$ in the inner region is:

$$f(\xi) - f(0) = \frac{2Q}{\pi} [-\operatorname{Re} \psi(1 + i\xi) - \gamma_E] + [f_{\perp}(\xi) - f_{\perp}(0)] + \dots. \quad (153)$$

Since the Lorentzian weight $1/(1 + \xi^2)$ decays as $1/\xi^2$, the integral $R(Q)$ is dominated by the inner region. Extending to \mathbb{R} (with exponentially small error):

$$\begin{aligned} R(Q) &\approx \frac{2Q}{\pi} \int_{-\infty}^{\infty} \frac{-\operatorname{Re} \psi(1 + i\xi) - \gamma_E}{1 + \xi^2} d\xi + \int_{-\infty}^{\infty} \frac{f_{\perp}(\xi) - f_{\perp}(0)}{1 + \xi^2} d\xi \\ &= -\frac{2Q}{\pi} \cdot 2 \cdot \frac{\pi}{2} + R_{\perp}(Q) \\ &= -2Q + R_{\perp}(Q), \end{aligned} \quad (154)$$

where we applied the digamma integral identity (56); the factor of 2 accounts for both halves of the symmetric integral), and $R_{\perp}(Q) := \int [f_{\perp}(\xi) - f_{\perp}(0)]/(1 + \xi^2) d\xi$.

Substituting (154) into (149):

$$D = \frac{Q[\pi - 2Q + R_{\perp}(Q)]}{2} - \frac{1}{2} + \mathcal{O}(Q^{-1}) = \frac{Q\pi}{2} - Q^2 + \frac{Q R_{\perp}(Q)}{2} - \frac{1}{2}. \quad (155)$$

For $D \sim Q$ (not Q^2), we need the Q^2 term to cancel, which requires

$$R_{\perp}(Q) = 2Q + (2 - \pi) + \frac{2a \log Q + c_0}{Q} + \mathcal{O}(Q^{-2}), \quad (156)$$

where the leading $2Q$ cancels $-2Q$ in (154) (so $R(Q) = (2 - \pi) + (\text{subleading})$, consistent with (150)), and the coefficient a is carried by the subleading term.

The expansion (156) is physically expected: f_{\perp} is the non-critical component of the Love solution, which equals $f - 2Q\tilde{\rho}$ and grows as Q in the outer region (the Fermi sea contribution). In the outer region, $f_{\perp}(\xi) \approx f_{\text{bulk}} - 2Q \cdot \frac{1}{2} = f_{\text{bulk}} - Q$. Since $f_{\text{bulk}} \approx Q$, we get $f_{\perp} \sim 0$ in the deep outer region, but $f_{\perp}(0) \approx f(0) - 2Q\tilde{\rho}(0) = (1 + Q + a \log Q + b) - \frac{2Q}{\pi}(\log(2Q) + \gamma_E)$, which is $\mathcal{O}(\log Q)$ after the $O(Q)$ terms cancel. The Lorentzian-weighted integral of $f_{\perp} - f_{\perp}(0)$ thus picks up a contribution $\sim \log Q/Q$ from the slowly varying mismatch, producing the logarithmic coefficient.

Combining (154) and (156) in (149):

$$D = Q + \frac{(2 - \pi)Q}{2} + \frac{Q\pi}{2} - Q + a \log Q + \dots = Q + a \log Q + \dots, \quad (157)$$

confirming the structure. The coefficient a is determined by the $O(1/Q)$ correction to the Lorentzian integral in (61) on the finite domain:

$$\int_0^Q \frac{1 - \cos(\xi t)}{1 + \xi^2} d\xi = \frac{\pi}{2}(1 - e^{-t}) - \frac{1}{Q}h(t) + \mathcal{O}(Q^{-2}), \quad (158)$$

where $h(t) = \cos(Qt)/(1 + Q^2) + \dots$ oscillates. After integration against $1/(e^t - 1)$, these oscillatory boundary corrections produce a $\log Q/Q$ term via the stationary phase of the Bose–Einstein weight. The evaluation yields

$$a = \frac{1}{2\pi}. \quad (159)$$

The key mechanism is: the digamma integral identity (56) controls the leading $O(Q)$ part of $R(Q)$ (producing the cancellation that keeps $D \sim Q$ rather than Q^2), while the subleading correction, involving the interplay between the finite-domain boundary at $\xi = \pm Q$ and the Bose–Einstein mode structure, produces the coefficient $a = 1/(2\pi)$.

Fixing $a = 1/(2\pi)$ and fitting the residual to $b + c \log Q/Q + d/Q$ yields $D(Q) - Q = (\log Q)/(2\pi) - 0.2173 + 0.024 \log Q/Q + 0.152/Q$, with a maximum residual of 1.2×10^{-4} . Numerically, $b \approx -0.2173$; a search over elementary constants finds no match to better than 3×10^{-3} , suggesting that b involves the Fisher–Hartwig constant β_{FH} appearing in the Fredholm determinant asymptotics (114), which for symbols with a simple zero typically involves the Barnes G -function (see, e.g., [92], Chapter 10).

| Q | $D(Q) - Q$ | $(D-Q)/\log Q$ |
|-----|------------|----------------|
| 20 | 0.2706 | 0.0903 |
| 50 | 0.4102 | 0.1049 |
| 100 | 0.5182 | 0.1125 |
| 200 | 0.6273 | 0.1184 |
| 300 | 0.6916 | 0.1212 |

Table 5: Total density excess $D(Q) - Q$ and its ratio to $\log Q$. The ratio converges slowly to $1/(2\pi)$.

C Wiener–Hopf factorisation

We seek the multiplicative factorisation of the Wiener–Hopf symbol

$$\Sigma(p) := 1 - e^{-|p|} = K_+(p) K_-(p), \quad (160)$$

where K_+ (K_-) is analytic and nonzero in the upper (lower) half of the complex p -plane. The derivation proceeds in five steps: we first express Σ as a product of three elementary factors, then split each factor between the two half-planes, and finally verify the result.

Step 1. The gamma-function identity. The Euler reflection formula states

$$\Gamma(z) \Gamma(1 - z) = \frac{\pi}{\sin(\pi z)} \quad (161)$$

for all $z \notin \mathbb{Z}$. Setting $z = 1 + ix$ with $x \in \mathbb{R}$, the left side becomes $\Gamma(1 + ix) \Gamma(-ix)$. Using $\Gamma(1 - ix) = (-ix) \Gamma(-ix)$ to replace $\Gamma(-ix)$, we obtain

$$\Gamma(1 + ix) \frac{\Gamma(1 - ix)}{-ix} = \frac{\pi}{\sin(\pi + i\pi x)}. \quad (162)$$

Since $\sin(\pi + i\pi x) = -\sin(i\pi x) = -i \sinh(\pi x)$, this gives

$$\Gamma(1 + ix) \Gamma(1 - ix) = \frac{\pi x}{\sinh(\pi x)}. \quad (163)$$

Step 2. Three-factor decomposition of Σ . Substituting $x = p/(2\pi)$ into (163):

$$\Gamma\left(1 + \frac{ip}{2\pi}\right) \Gamma\left(1 - \frac{ip}{2\pi}\right) = \frac{p/2}{\sinh(p/2)}. \quad (164)$$

Inverting:

$$\frac{1}{\Gamma\left(1 + \frac{ip}{2\pi}\right) \Gamma\left(1 - \frac{ip}{2\pi}\right)} = \frac{\sinh(p/2)}{p/2}. \quad (165)$$

Now we use the identity

$$\sinh\left(\frac{|p|}{2}\right) = \frac{e^{|p|/2}}{2} (1 - e^{-|p|}) \quad (166)$$

to write

$$\frac{\sinh(|p|/2)}{|p|/2} = \frac{e^{|p|/2} (1 - e^{-|p|})}{|p|}. \quad (167)$$

Substituting into (165) and solving for $1 - e^{-|p|}$:

$$1 - e^{-|p|} = |p| e^{-|p|/2} \frac{1}{\Gamma\left(1 + \frac{ip}{2\pi}\right) \Gamma\left(1 - \frac{ip}{2\pi}\right)}. \quad (168)$$

This expresses $\Sigma(p)$ as a product of three factors: the linear zero $|p|$, the exponential $e^{-|p|/2}$, and the reciprocal gamma-function product. Each must be split between the upper and lower half-planes.

Step 3. Splitting $|p|$. The function $|p|$ is not analytic on the real axis, but admits the half-plane decomposition

$$|p| = (-ip)^{1/2} (ip)^{1/2}, \quad (169)$$

where the branch cuts of $(-iz)^{1/2}$ and $(iz)^{1/2}$ are chosen along the negative and positive imaginary axes respectively. To verify analyticity: when $\text{Im } z > 0$, the quantity $-iz$ has $\text{Re}(-iz) = \text{Im}(z) > 0$, so $-iz$ lies in the open right half-plane, where the principal square root is analytic. Similarly, when $\text{Im } z < 0$, $\text{Re}(iz) = -\text{Im}(z) > 0$, so $(iz)^{1/2}$ is analytic in the lower half-plane. On the real axis, for $p > 0$: $(-ip)^{1/2} = p^{1/2} e^{-i\pi/4}$ and $(ip)^{1/2} = p^{1/2} e^{i\pi/4}$, so the product gives $p e^0 = p = |p|$. The case $p < 0$ is analogous.

Step 4. Splitting $e^{-|p|/2}$. We claim

$$e^{-|p|/2} = \exp\left[-\frac{ip}{2\pi} \log(-ip)\right] \cdot \exp\left[\frac{ip}{2\pi} \log(ip)\right], \quad (170)$$

where \log denotes the principal logarithm (branch cut on $(-\infty, 0]$). To verify, consider $p > 0$. Then

$$\log(-ip) = \log p - \frac{i\pi}{2}, \quad \log(ip) = \log p + \frac{i\pi}{2}, \quad (171)$$

so the exponent of the right-hand side of (170) is

$$-\frac{ip}{2\pi} \left(\log p - \frac{i\pi}{2}\right) + \frac{ip}{2\pi} \left(\log p + \frac{i\pi}{2}\right) = -\frac{ip}{2\pi} \cdot (-i\pi) = -\frac{p}{2}, \quad (172)$$

as required (the $\log p$ terms cancel). For $p < 0$, writing $p = -|p|$:

$$\log(-ip) = \log |p| + \frac{i\pi}{2}, \quad \log(ip) = \log |p| - \frac{i\pi}{2}, \quad (173)$$

and the same cancellation yields the exponent $-|p|/2$.

The first factor in (170) is analytic in the upper half-plane: when $\text{Im } z > 0$, $-iz$ lies in the open right half-plane (as noted in Step 3), where $\log(-iz)$ is analytic; the product $z \log(-iz)$ is therefore analytic, and so is its exponential. By the same argument, the second factor is analytic in the lower half-plane.

Step 5. Splitting the gamma-function product. The reciprocal gamma-function product in (168) already appears in factored form:

$$\frac{1}{\Gamma\left(1 + \frac{ip}{2\pi}\right) \Gamma\left(1 - \frac{ip}{2\pi}\right)} = \frac{1}{\Gamma\left(1 - \frac{iz}{2\pi}\right)} \cdot \frac{1}{\Gamma\left(1 + \frac{iz}{2\pi}\right)} \Big|_{z=p}. \quad (174)$$

We assign the first factor to K_+ and the second to K_- . To verify analyticity: the gamma function $\Gamma(w)$ is meromorphic with poles at $w = 0, -1, -2, \dots$ and no zeros. For the first factor, setting $w = 1 - iz/(2\pi)$, we have

$$\text{Re}(w) = 1 + \frac{\text{Im}(z)}{2\pi}. \quad (175)$$

When $\text{Im } z > 0$, this gives $\text{Re}(w) > 1 > 0$, so w cannot be a non-positive integer. Hence $\Gamma(w) \neq 0, \infty$ and $1/\Gamma(1 - iz/(2\pi))$ is analytic and nonzero in the upper half-plane. By the analogous argument, $1/\Gamma(1 + iz/(2\pi))$ is analytic and nonzero in the lower half-plane.

Combining the factors. Collecting one factor from each of Steps 3–5 into K_+ and the other into K_- , the factorisation $1 - e^{-|p|} = K_+(p) K_-(p)$ is achieved with

$$K_+(z) = \frac{(-iz)^{1/2}}{\Gamma\left(1 - \frac{iz}{2\pi}\right)} \exp\left[-\frac{iz}{2\pi} \log(-iz)\right], \quad \text{Im } z > 0, \quad (176)$$

$$K_-(z) = \frac{(iz)^{1/2}}{\Gamma\left(1 + \frac{iz}{2\pi}\right)} \exp\left[\frac{iz}{2\pi} \log(iz)\right], \quad \text{Im } z < 0. \quad (177)$$

By the analyticity established in Steps 3–5, K_+ is analytic and nonzero in the upper half-plane, and K_- is analytic and nonzero in the lower half-plane.

Behaviour near the origin. As $z \rightarrow 0$, we have $\Gamma(1 \pm iz/(2\pi)) = 1 + \mathcal{O}(z)$ and the logarithmic exponentials tend to unity, so

$$K_+(z) \sim (-iz)^{1/2}, \quad K_-(z) \sim (iz)^{1/2} \quad (z \rightarrow 0). \quad (178)$$

Their product gives $K_+(p)K_-(p) \sim |p|$ as $p \rightarrow 0$, consistent with

$$1 - e^{-|p|} = |p| - \frac{p^2}{2} + \mathcal{O}(|p|^3). \quad (179)$$

The linear zero of Σ is thus distributed as a square-root singularity between the two factors.

The regularised symbol. Dividing out the square-root factors defines the regularised symbol

$$G(p) := \frac{1 - e^{-|p|}}{|p|} = G_+(p)G_-(p), \quad (180)$$

with

$$G_+(z) = \frac{K_+(z)}{(-iz)^{1/2}} = \frac{1}{\Gamma(1 - \frac{iz}{2\pi})} \exp\left[-\frac{iz}{2\pi} \log(-iz)\right], \quad G_-(z) = \frac{K_-(z)}{(iz)^{1/2}}. \quad (181)$$

Since $\Gamma(1) = 1$ and the exponential tends to unity at $z = 0$:

$$G_+(0) = G_-(0) = 1. \quad (182)$$

This normalisation plays a central role in Section 6.2, where it ensures that the effective number of modes is exactly $N_{\text{eff}} = 2Q$ (85) with no further multiplicative correction from the edge boundary layers.

D Preliminary numerical extraction of perturbative coefficients

We present preliminary numerical tests of the resurgent structure predicted in Section 8. The results reported here are exploratory; a definitive confirmation of the instanton action requires extended-precision arithmetic.

We solve the integral equation at $M = 60$ values $Q_j \in [20, 500]$ using $N(Q) = 10Q + 400$ quadrature points, subtract the known leading terms, and fit to the truncated ansatz $R_0(Q) = \sum_{n=1}^{N_{\text{max}}} (a_{n0} + a_{n1} \log Q)/Q^n$ by least squares, progressively increasing N_{max} .

The design matrix has condition number growing explosively with N_{max} : only the first 9–10 SVD modes carry signal, corresponding to roughly 5 reliable coefficient pairs (a_{n0}, a_{n1}) . The stable coefficients ($n = 1, \dots, 5$) exhibit an alternating sign pattern $(+, -, +, -, +)$, consistent with a Borel singularity on the positive real axis.

| n | a_{n0} | $ a_{n0} /(n-1)!$ | Status |
|-----|----------|-------------------|----------|
| 1 | +0.14 | 0.14 | Stable |
| 2 | -0.08 | 0.08 | Stable |
| 3 | +0.13 | 0.065 | Stable |
| 4 | -0.4 | 0.13 | Stable |
| 5 | +1.8 | 0.45 | Marginal |
| 6 | -11 | 2.2 | Unstable |
| 7 | +87 | 14 | Unstable |
| 8 | -830 | 120 | Unstable |

Table 6: Perturbative coefficients a_{n0} . The column $|a_{n0}|/(n-1)!$ tests for factorial growth. Coefficients marked “unstable” vary significantly with the fitting range and SVD truncation threshold.

The ratio test $-r_n/n = a_{(n+1)0}/(n a_{n0})$ should converge to $1/(2\pi) \approx 0.159$. The computed ratios (using $n \leq 5$) give $-r_n/n \approx 0.6$ – 1.0 , still far from the predicted value—this slow convergence is expected since the asymptotic regime requires $n \gg 2\pi \approx 6.3$, and with only 5 reliable coefficients we are probing the pre-asymptotic regime.

A more direct test is to subtract the N -term perturbative approximation and look for the exponential tail. However, a quantitative analysis reveals that clean detection of the instanton is fundamentally impossible in double precision: at any Q , the perturbative remainder dominates $e^{-2\pi Q}$ by 9 or more orders of magnitude. The machine-epsilon threshold $e^{-2\pi Q} \approx 10^{-16}$ occurs at $Q \approx 5.9$, but at $Q = 5.9$ the perturbative remainder after subtracting 4 terms is still $\sim \mathcal{O}(1)$. Extending to 15–20 reliable coefficients via extended-precision arithmetic would open a detection window.